NASA Contractor Report 4302

An Unsteady Lifting Surface Method for Single Rotation Propellers

Marc H. Williams
Purdue University
West Lafayette, Indiana

Prepared for
Lewis Research Center
under Grant NAG3-499

National Aeronautics and
Space Administration
Office of Management
Scientific and Technical
Information Division

1990

Preface

This report is a somewhat modified and expanded version of a report issued in June 1985 by the School of Aeronautics and Astronautics at Purdue University entitled 'An Unsteady Lifting Surface Theory for Single Rotation Propellers' [13]. The report provides background on a code, UPROP3S, that has been developed for the unsteady aerodynamic and aeroelastic analysis of advanced turboprops. Further information on the use of that code is given in a user's manual [14]. The treatment of the blade boundary condition in Sec 3.1 has been altered from its original form, which was slightly in error. In addition, new sections on mistuning (Sec 1.4) and aeroelastic analysis (Appendix VI) have been added. The aerodynamic code based on this report has been incorporated into the aeroelastic analysis program ASTROP3 at NASA Lewis Research Center. However, the aeroelastic analysis given in App. VI is the one used in the code UPROP3S, and was not used in ASTROP3. Since the scheme has not been described elsewhere, a brief outline has been included herein.

Contents

Nomenclature

C_{ij} Aerodynamic influence coefficient, Eq.(28)

C_{L_D} design lift coefficent of 16 series airfoils, Eq.(48)

C_T Thrust coefficient, Eq.(45)

C_p Power coefficient, Eq.(46)

$D_\pm$ panel edge integrals, Eq.(30)

D_0 part of $D_\pm$ from K_0

D_1 part of $D_\pm$ from K_1, Eq.(33)

H Heaviside step function

i $\sqrt{-1}$

J advance ratio , π/S

K propeller kernel function, Eq.(II.15)

K_0 quasi planar kernel function, Eq.(37)

K_1 residual kernel function , $K - K_0$

$\vec{L}$ normal to helical surface , Eq.(5)

m interblade phase index, Eq.(20)

M_x axial Mach number

M_0 Helical Mach number of a blade point

$\vec{n}$ unit normal to blade surface

N_B number of blades or periodic groups of blades

P scaled pressure difference across surface, Eq.(24)

Q_{ij} generalized aerodynamic force, Eq.(50)

r_h blade hub radius

r_t blade tip radius

$\vec{R}$ blade surface rotation, Eq.(19)

S tip to axial speed ratio, $\Omega r_t/U$

t time

$\vec{u}$ perturbation velocity of fluid

U axial flow velocity

v_n normal velocity of blade surface, Eq.(11)

V side slip velocity

W scaled upwash on blade surface, Eq.(24)

x axial distance along axis of rotation, undisturbed air frame

$\bar{x}$ axial coordinate in rotor frame, Eq.(2), Fig.1

y cartesian nonrotating frame coordinate

$\bar{y}$ cartesian rotating frame coordinate, Eq.(2), Fig.1

z cartesian nonrotating frame coordinate

$\bar{z}$ cartesian rotating frame coordinate (along pitch change axis)

Greek symbols

α blade helical curvature , Eq.(6)

β angle between blade chord and plane of rotation

$\beta_{3/4}$ blade setting angle at 3/4 tip radius

$\Delta\theta_B$ angle between blades

Δp front - back pressure difference

$\vec{\delta}$ blade surface displacement

δ normal component of $\vec{\delta}$, Eq.(16)

η efficiency, Eq.(47)

θ circumferential angle (nonrotating frame)

$\bar{\theta}$ circumferential angle (rotating frame)

ε control point position in fraction of panel chord

ξ fraction of blade chord from leading edge

ρ_0 undisturbed air density

$\sigma(r)$ blade surface helical coordinate, Eq.(4)

ω vibration, or excitation frequency

$\bar{\omega} = \omega/\Omega$

Ω rotational velocity (positive in - θ direction)

Section 1
Theory

(1.1) *Introduction*

When a propeller undergoes blade vibration or operates in a nonuniform stream, unsteady aerodynamic forces are exerted on the blades. These fluctuating forces may influence the fatigue life, the aeroelastic stability and the noise output of the propeller. It is essential, therefore, to be able to predict aerodynamic responses for propellers in time dependent flows. This report describes a numerical method for making such predictions for single rotation propellers.

The analytical model employed herein uses linear compressible small disturbance theory. In practice this means that the blades must be thin and at small local angles of attack (below stall). Further, any incident flow distortions must involve velocities which are small compared to the helical blade speed. Finally, linear theory does not account for embedded shocks which can occur on transonic tips or in a blade passage (at high solidity, where blockage may be significant).

In addition to linearity, we assume that the load at any point on a blade fluctuates harmonically in time with some prescribed frequency ω. Hence the entire disturbance field will fluctuate harmonically at the same frequency (in a frame rotating with the propeller). More complex periodic disturbances can, of course, be examined by breaking the disturbance into its Fourier components and finding the response to each individually.

A blade may be thought of as a mean camber surface overlaid with a thickness distribution. In the linear approximation the thickness distribution does not effect the loads and will, therefore, be ignored. The mean camber surface, which determines the loads, may be either rigid or may vibrate harmonically about some average position. In either case the object of the calculation is to find that load distribution (pressure jump across the surface) for which there is no flow through the surface.

The task of finding such a load distribution is simplified by transferring the boundary conditions from the actual camber surface to a neighboring helical surface (see Sec. 1.3). This is done by choosing some curve, called the "generator," on the surface. If the blade vibrates, the generator is chosen to lie on the average camber surface. As the blade advances and rotates the generator sweeps out a fixed helical surface. If the actual blade lay exactly on the helical surface - and there were no incident flow nonuniformities - then the blade would produce no disturbance as it slices through the air. Thus it is the deviation of the camber surface from the helical surface swept out by the generator which produces a load.

In practice, the load distribution is placed on the helical surface, rather than on the camber surface. The advantage of this transfer is that the trajectories of all points at a fixed radius on the helical surface are the same. Since, as will be seen later, the

calculation of the velocity induced by one load point on the blade requires an integration along the trajectory of that point, the present scheme allows one integration to serve all blade points at a fixed radius. If the load distribution were placed on the camber surface then a separate trajectory integral would need to be done for each blade point.

In this model, then, a propeller blade is thought of as a distributed load sliding along the helical surface which induces a given distribution of normal velocities on itself (Sec. 1.3).

Linear aerodynamic theory provides an explicit expression for the normal velocity at any point in terms of a surface integral of the load distribution. Since the velocity is given, this relation amounts to a linear integral equation for the load (Sec. 1.5). To solve this integral equation the blade is broken into a finite number of elements, on each of which the load is considered to be constant. To each element a control point is assigned at which the normal velocity is specified. The loads on all the elements are then determined simultaneously by requiring that their resultant induced normal velocity have the specified value at each control point.

The principle difficulty in implementing this scheme is that the velocity field induced by a constant load blade element cannot be computed exactly. In fact, not even the velocity induced by a point load can be computed exactly (meaning, of course, that evaluating either quantity to machine accuracy would require excessive computation times). Hence the influence coefficients (the normal velocity at a control point induced by a unit load on an element), must be approximated numerically with enough accuracy to make the results meaningful yet with enough simplicity to make the scheme practical. The way in which the influence coefficients are calculated is the key to making the method work. The scheme used for the present calculations is described in detail in Chapter 1.6.

Several three dimensional linear lifting surface theories for propellers, similar in various respects to the present method, have appeared in the past. The work of Hammond et al. [1] is closest to the present scheme, differing only in the discretization procedure. Hanson [2] uses the same theoretical framework but expresses the kernel function as an infinite series of Bessel functions. He gives the equations, but no results, for a vibrating blade. Farassat [3] and Long [4], employ linear compressible theory, as does the present work, but do not use the mean surface approximation. Like Hanson, they show no results for a vibrating blade. Sullivan and co-workers [5-6] have developed a vortex lattice method for steady performance calculations (recently extended to counter-rotation, using a quasi-steady approximation [7]. Finally we note that a number of 3-D finite difference algorithms have been developed for the steady problem [8], though none has been extended to unsteady flows.

(1.2) *Coordinates and Geometry*

Coordinate Systems

(see Fig. (1))

(a) Inertial Frame

(x,y,z) is a right handed cartesian system fixed in the undisturbed fluid. In this frame the propeller center of rotation advances with speed U along the (-x) axis and the blades rotate, clockwise, at speed Ω when viewed from the -x axis (so the rotational velocity vector points along the +x axis).

(x, r, θ) are cylindrical coordinates, with θ measured from the z-axis; so that:

$$y = r \sin\theta, \quad z = r \cos\theta \tag{1}$$

(b) Rotor Frame

($\bar{x}$, $\bar{y}$, $\bar{z}$) is a right handed cartesian system fixed in the rotor. (The $\bar{z}$ axis can be taken to coincide with the pitch change axis of the reference blade).

($\bar{x}$, r, $\bar{\theta}$) are cylindrical coordinates fixed in the rotor.

From the sign convention adopted we have,

$$\bar{x} = x + Ut\,, \quad \bar{\theta} = \theta + \Omega t$$

$$\bar{y} = r \sin\bar{\theta}\,, \quad \bar{z} = r \cos\bar{\theta} \tag{2}$$

Helical Surface

(see Fig. (2))

Any fixed point on a blade follows a helical trajectory $x - U/\Omega\,\theta = \bar{x} - U/\Omega\,\bar{\theta}$.

Let $\bar{x}_g(r)$, $\theta_g(r)$ define some space curve lying on the blade chord surface (*e.g.* The trailing edge or mid-chord line). This curve generates a helical surface,

$$x = U/\Omega\,(\theta + \sigma) \tag{3}$$

where

$$\sigma(r) \equiv \Omega/U\,\bar{x}_g - \bar{\theta}_g\,. \tag{4}$$

Note that this helical surface is time-independent, and fixed by the advance ratio and the choice of generator curve (which determines $\sigma(r)$).

The normal to the helical surface is,

$$\vec{L} = \nabla(x - U / \Omega (\theta + \sigma))$$

$$= \vec{i}_x - U / (\Omega r) (\vec{i}_\theta + \alpha \vec{i}_r) \tag{5}$$

where $(\vec{i}_x, \vec{i}_\theta, \vec{i}_r)$ are unit vectors in the (x, θ, r) directions respectively, and

$$\alpha = r \frac{d\sigma}{dr} . \tag{6}$$

Note that the normal $\vec{L}$ is a function of position only.

We shall parameterize the helical surface by (r, θ). An area element on the surface is, then,

$$d\vec{A} = \vec{L}\, r dr\, d\theta \tag{7}$$

and an element of arc length along the surface at fixed radius is,

$$ds = d\theta\, [r^2 + (U/\Omega)^2]^{.5} \tag{8}$$

In the aerodynamic model, the load distribution is placed on the helical surface, within the region

$$r_h \le r \le r_t \tag{9}$$

$$\bar{\theta}_{LE}(r) \le \bar{\theta} \le \bar{\theta}_{TE}(r) .$$

These edge coordinates of the lifting surface are obtained by projecting the blade chordline onto the helical surface so that the (helical) arc lengths are equal:

$$\bar{\theta}_{TE} - \bar{\theta}_{LE} = \left[\frac{(\Delta x)^2 + (r\Delta\theta)^2}{(U/\Omega)^2 + r^2} \right]^{1/2} \tag{10}$$

(1.3) *Surface Boundary Condition*

The normal velocity of the fluid at the blade surface must equal the normal velocity of the blade surface at every point. Let $\vec{u}$ be the fluid velocity in the inertial frame (*i.e.* relative to the undisturbed fluid), $\vec{n}$ the unit normal to the blade surface, and v_n the normal velocity of the blade surface (again in the inertial frame). Then at every point on the blade we must have,

$$\vec{n}\cdot\vec{u} = v_n \ . \tag{11}$$

In the present (linearized) model, wherein the load is transferred to the helical surface, the boundary condition is similarly transferred. Thus at every point on the helical surface we impose the constraint,

$$\vec{L}\cdot\vec{u} = |\vec{L}|\, v_n \ , \tag{12}$$

which says that the normal velocity induced on the helical surface by the load distribution must equal v_n (which is known once the blades shape and motion are specified).

In the present study the normal velocity is assumed to be either steady or simple harmonic at any fixed blade point. Expressions for three cases will be given here: steady operation, propeller in yaw, and blade vibration.

Steady Operation

For steady state operation we have,

$$v_n = -U n_x - \Omega(\bar{z}\, n_y - \bar{y} n_z) \ , \tag{13}$$

(where n_x, n_y, n_z are the components of $\vec{n}$ in the blade coordinate system).

Blade in Yaw

If the propeller blades are rigid but operate in a crosswind V (in the y direction), the corresponding amplitude of v_n (on the reference blade) is:

$$v_n = -V\,(n_y + i\, n_z) \ . \tag{14}$$

The fluctuating frequency is $\omega = \Omega$ and the interblade phase index is m = -1 (see "periodicity".) This case is equivalent to a yaw angle of $\tan^{-1} V / U = V / U$. Of course, the yaw angle must be small in order for linear theory to be applicable, in which case the resultant blade loads will be proportional to the yaw angle.

Blade Vibration

If the blades vibrate with frequency ω, the amplitude of the resulting normal velocity fluctuation may be computed from the displacement vector $\vec{\delta}$ and rotation vector

$\vec{R}$ assigned to each blade point $\vec{x}$:

$$v_n = i\omega\delta + v_R \tag{15}$$

where

$$\delta = \vec{n}\cdot\vec{\delta} \tag{16}$$

is the normal displacement, and $v_R = v_{R_1} + v_{R_2}$, with

$$v_{R_1} = U\,(\,n_y R_z - n_z\,R_y\,) \tag{17}$$

$$+\,\Omega[(\bar{z}\,n_z + \bar{y}\,n_y)R_x - n_x(\bar{y}\,R_y + \bar{z}\,R_z)]$$

being the contribution from rotational deformation, and

$$v_{R_2} = \Omega\,(\,\delta_y\,n_z - \delta_z\,n_y\,) \tag{18}$$

being the contribution from the increase in speed due to a radial displacement (which was missing in the original report and code.)

These expressions can be used directly if the structural displacement and rotation vectors are available (e.g. from a finite element analysis). If the rotation vectors are not available (or are unreliable), they can be computed from their fundamental definition in terms of derivatives of $\vec{\delta}$,

$$R_x = -n_y\,\vec{n}\cdot\vec{\delta}_z + n_z\,\vec{n}\cdot\vec{\delta}_y \tag{19}$$

$$R_y = n_x\,\vec{n}\cdot\vec{\delta}_z$$

$$R_z = -n_x\,\vec{n}\cdot\vec{\delta}_y$$

The subscripts on $\vec{\delta}$ denote differentiation along the indicated directions, assuming the blade is parameterized by y and z.(This method of computing rotation vectors was not used in the original work and is superior to the scheme described earlier.)

In practice, the blade is usually defined by a discrete set of nodes covering the camber surface, with $\vec{x}$, $\vec{\delta}$, and ,perhaps, $\vec{R}$ defined at each node. To determine the normal velocity at any prescribed point on the surface, the $\vec{x}$ data is fit with a polynomial (quadratic in y and bilinear in z and y) ,least squares interpolated to the six nearest neighbor nodes. The five coefficients of this surface fit can be used to define the surface normals as well as the interpolations of the displacement vector and its derivatives.

(1.4) *Periodicity*

We assume that there are N_B identical blades (j=1, ..., N_B) spaced equally in angle increments $\Delta\bar{\theta}_B = 2\pi/N_B$. Then the load on any one blade will be the same as the load on every other blade except for possible phase shifts. To allow for such phase shifts we assume that the normal velocity on the jth blade at a given point is related to the normal velocity on the reference blade (j = 1) at the corresponding point by,

$$(v_n)_j = (v_n)_i \, e^{im(j-1)\Delta\bar{\theta}_B} \tag{20}$$

where m may assume any integer value, m = 0, 1, ..., N_B-1.

Let Δp be the pressure difference (upwind-downwind) across a blade. Then, by (17), the loads are also related by

$$(\Delta p)_j = (\Delta p)_1 \, e^{im(j-1)\Delta\bar{\theta}_B} \, , \tag{21}$$

so that only the load on the reference blade need be found.

Note that with N_B blades there will be N_B helical surfaces with helix numbers (Eq.(4)) given by,

$$\sigma_j = \sigma_1 - (j-1)\,\Delta\bar{\theta}_B \tag{22}$$

Finally we shall assume that the normal velocity and load at any fixed point on a blade vary harmonically in time, with frequency ω, like $e^{i\omega t}$. For most interference problems ω will be a harmonic of the rotor frequence Ω. For vibration problems, ω will be close to a blade natural frequency.

Mistuning

The foregoing discussion is easily extendible to cases in which not all the blades are identical, but the 'mistuning' is distributed periodically(eg. alternate mistuning.) This is done simply by redefining 'blade' to mean 'a group of blades'. The groups are assumed to be indistinguishable, but each group may consists of an arbitrary collection of disjoint surfaces. (The only special coding change that was needed to allow for different blades within a group was to ensure that the tip of one blade was not connected by panels to the root of the next blade.) If all the blades are different (i.e. there is no periodicity) then there is ,by definition, only one group. A 'tuned' rotor consists of N_B groups with one blade per group. Alternate mistuning would have N_B groups with two blades per group.

In addition, mistuning studies require a generalization of 'blade mode'. The simplest definition of a 'group mode' is to suppose that one group mode corresponds to one blade in the group vibrating in one of its natural modes while all other blades in the

group remain fixed. Thus the total number of group modes will be the number of modes retained per blade summed over the group. The numbering sequence is arbitrary.

(1.5) *Lifting Surface Integral Equation*

From the assumptions of aerodynamic linearity, simple harmonic time dependence, and blade to blade periodicity, the entire disturbance field surrounding the propeller can be determined directly from the distribution of load amplitude over the reference blade. In particular, then, the load distribution determines the distribution of normal velocity over the reference blade.

This relationship between load and normal velocity can be expressed as an integral equation,

$$W(\bar{r}, \bar{\theta}) = \int_{\bar{r}_h}^{1} \int_{\bar{\theta}_{LE}}^{\bar{\theta}_{TE}} P(\bar{r}_o, \bar{\theta}_o) \frac{\partial}{\partial \bar{\theta}} K(\bar{\theta}-\bar{\theta}_o, \bar{r}, \bar{r}_o) \bar{r}_o d\bar{\theta}_o d\bar{r}_o \tag{23}$$

where

$$W = 4\pi \left(\frac{\vec{L}\cdot\vec{u}}{U}\right) e^{i\bar{\omega}\bar{\theta}}$$

$$P = S^2 \frac{\Delta p}{\rho_o U^2} e^{i\bar{\omega}\bar{\theta}_o} . \tag{24}$$

Here W is proportional to the normal velocity, P to the pressure jump across the blade, and K is a (known) kernel function. In most applications the normal velocity is specified and the integral equation must then be solved for the load distribution. The method used to do this will be described in subsequent sections.

Expressions for the kernel function are derived in Appendices I and II. Here we will only discuss its general properties.

Parametrically, K depends on the speed ratio, S; the frequency ratio, $\bar{\omega} = \omega/\Omega$; the axial Mach number, M_x; the interblade phase index, m; the number of blades, N_B; and the helix numbers, $\sigma(r)$. If these quantities are specified then K is uniquely determined. The kernel does not depend on the blade planform shape or the normal velocity distribution.

Physically, K can be interpreted as follows. Suppose that the load is concentrated on a particular radius, with zero amplitude upstream and constant amplitude downstream:

$$P(\bar{r}, \bar{\theta}) = H(\bar{\theta})\delta(\bar{r}-\bar{r}_o)/\bar{r}_o . \tag{25}$$

If there are N_B blades then there are N_B such loaded lines, all extending from the same axial position to downstream infinity, with equal strengths but phase shifted in accord with the index, m. The normal velocity induced by this set of loaded lines on the reference blade is, from Eq's. (23) and (25),

$$W(\bar{r}, \bar{\theta}) = K(\bar{\theta}, \bar{r}, \bar{r}_o) . \tag{26}$$

The kernel depends only on the angle difference $\bar{\theta} - \bar{\theta}_o$, because of rotational symmetry. It depends on the radii r, r_o separately, because the relative velocity is a function of radius. The evaluation of K as a function of $\bar{\theta} - \bar{\theta}_o$ for any specified pair of radii r, r_o, requires numerical integration along the N_B helical lines at radius r_o (the integration is a consequence of Newton's law - velocity is the integral of the force producing it). As a result the evaluation of K tends to be the dominant part of the load calculation for moderate panel density. When the number of panels is very large the $O(n^3)$ cost of Gaussian elimination will dominate.

From the physical interpretation of K as the velocity induced by a set of line loads it is apparent that K will contain singularities. In particular, K will always be infinite on $r = r_o$, $\bar{\theta} > \bar{\theta}_o$, i.e. on the loaded line. If the helical Mach number at radius r_o is less than one then K will be bounded everywhere else. However, if the helical Mach number is greater than one, then a spiral Mach cone will extend back from the tip of each of the loaded lines. Thus K will be infinite wherever one of these Mach cones intersects the reference helical surface. The singularities of K must be handled very carefully in constructing a numerical solution of the lifting surface integral equation.

(1.6) *Discretization of the Integral Equation*

In brief, the lifting surface integral equation, Eq(23), is solved approximately by splitting the blade into a finite number of elements within each of which P is assumed constant. The normal velocity W is then specified at one point per element, thereby reducing the integral equation to a set of simultaneous algebraic equations for the loads on each element.

More specifically, the blade is split into NRP radial strips of arbitrary width. Each strip is then divided into NXP chordwise pieces by a sequence of constant partial chord lines (the chordwise spacing is arbitrary). The blade is thereby decomposed into NP = NRP·NXP quadrilateral panels.

A control point is placed on each panel at its mean radius, a distance $\varepsilon\Delta\bar{\theta}$ downstream from the midspan panel leading edge, (where $\Delta\bar{\theta}$ is the panel chord at midspan , and distance is measured in θ.) The arrangement is illustrated in Fig. (3). The selection of ε is discussed in Sec. (2.2).

The algebraic system resulting from this discretization is

$$W_i = \sum_{j=1}^{NP} C_{ij} P_j \tag{27}$$

where

$$W_i = W \text{ at ith control point, } (\bar{\theta}_i, \bar{r}_i)$$

$$P_j = P \text{ on jth panel,}$$

$$C_{ij} = -\iint \frac{\partial K(\bar{\theta}_i - \bar{\theta}_o\ ,\ \bar{r}_i\ ,\ \bar{r}_o\ )}{\partial\bar{\theta}_o}\, d\bar{\theta}_o \bar{r}_o d\bar{r}_o \tag{28}$$

Note that the chordwise integration in the influence coefficient C_{ij} can be performed directly (this is why P, rather than Δp, was treated as being constant over the panel).

Hence

$$C_{ij} = D_- - D_+ \tag{29}$$

where $D_\pm$ are the radial integrals along the panel leading (-) and trailing (+) edges

$$D_\pm = \int K(\bar{\theta}_i - \bar{\theta}_{o\pm}, \bar{r}_i, \bar{r}_o)\bar{r}_o d\bar{r}_o \tag{30}$$

($\bar{\theta}_{o\pm}(\bar{r}_o)$ are the panel leading and trailing edge coordinates). Note that for a fixed control point, D_+ for one panel is the same as D_- for the next panel in the row. Thus D must be evaluated NXP+1 times per radial strip.

(1.6.1) *Numerical Evaluation of Influence Coefficients*

Computing an influence coefficient requires a radial integration of the kernel function for D. However, the kernel function evaluation itself must be done numerically so that only a few values of K will be available near any given panel. This is not a large problem, if the panels are small, unless the panel encloses, or lies near a singularity of the kernel. This does happen, however, when the control point radius lies within, or near, the panel row.

To circumvent at least some of the difficulties associated with the kernel function singularity, the kernel is split into two parts

$$K = K_o + K_1 \tag{31}$$

with a corresponding decomposition of D:

$$D = D_o + D_1 \ . \tag{32}$$

The K_o term is an analytical approximation which is valid when $r-r_o$ is small, and therefore contains the dominant part of the singular structure of K (to be precise, K and K_o behave like $(r-r_o)^{-2}$ near $r = r_o$ when $\bar{\theta} > \bar{\theta}_o$). The residual kernel, K_1, is simply defined as $K-K_o$. For the cases run, K_1 has been found to be also singular, but only as $(r-r_o)^{-1}$. This singularity will be accounted for in the evaluation of D_1.

The specific form of K_o used here will be given in the next section. The significant point is that it is simple enough that D_o can be evaluated exactly and efficiently.

The part of the influence coefficient arising from the residual kernel K_1, i.e., D_1, is evaluated by simple quadrature rules. The specific rule used depends on whether the control point lies within the panel row or not. (Cases (a) and (b) below)

Let the upper and lower radii of the panel be R_1 and R_2 respectively and suppose the particular panel edge in question runs from $\bar{\theta}_{o1}$ to $\bar{\theta}_{o2}$ (see Fig. 3). Then the value of D_1 required is:

$$D_1 = \int_{R_1}^{R_2} K_1(\bar{\theta} - \bar{\theta}_o, \bar{r}, \bar{r}_o)\bar{r}_o \, d\bar{r}_o \ . \tag{33}$$

(a) $\bar{r} \neq (R_1+R_2)/2 \equiv R_m$

In this case the control point is outside the panel row. The kernel K_1 is evaluated numerically along the midspan and D_1 is evaluated from

$$D_1 \equiv R_m(R_2 - R_1)K_1(\bar{\theta} - \bar{\theta}_{om}, \bar{r}, R_m)\cdot Q \tag{34}$$

where R_m and $\bar{\theta}_{om}$ are the mid-points as shown in Fig. 3. If $\bar{\theta} < \bar{\theta}_{om}$, i.e. if the control point is upstream from the panel edge, then the factor Q is set to 1. If $\bar{\theta} > \bar{\theta}_{om}$, though, the residual kernel K_1 has a pole at $\bar{r}_o = \bar{r}$ which may be close by. In this case we take

$$Q = \frac{R_m - \bar{r}}{R_2 - R_1} \int_{R_1}^{R_2} \frac{d\bar{r}_o}{\bar{r}_o - \bar{r}}$$

$$= \frac{R_m - \bar{r}}{R_2 - R_1} \ln \left| \frac{R_2 - \bar{r}}{R_1 - \bar{r}} \right| . \qquad (35)$$

If the control point radius is more than one or two panel spans removed, this correction factor is nearly one. It differs from one significantly only in the neighborhood; e.g. if $\bar{r} = R_m + R_2 - R_1$ then $Q = 1.1$.

(b) $\bar{r} = R_m$

In this case the control point is in the panel row and the kernel is singular along the midspan. The kernel is then evaluated numerically along the edges R_1 and R_2 and D_1 is evaluated from the quadrature rule:

$$D_1 = (R_2 - R_1) \frac{1}{2} R_m [K_1(\bar{\theta} - \bar{\theta}_{o2}, \bar{r}, R_2) + K_1(\bar{\theta} - \bar{\theta}_{o1}, \bar{r}, R_1)] \qquad (36)$$

Note that this rule is exact if $K_1 = a/(\bar{r}_o - \bar{r})$ (i.e. it gives $D_1 = 0$) and if K_1 is linear in $\bar{r}_o$.

In summary, if the control point lies outside the panel row we evaluate the residual kernel along the midspan of the row. If the control point lies within the row then we evaluate K_1 along the outer edges of the row. For each control point and panel row we will need numerical values for K_1 at a discrete set of angles $\bar{\theta} - \bar{\theta}_o$, numbering roughly $(NXP)^2$. In practice a single table of K_1 values covering the needed range of $\bar{\theta} - \bar{\theta}_o$ is generated for each panel and control point row and values for specific panels and control points are found by interpolation in the table.

(1.6.2) *The Quasi-Planar Kernel,* K_o

As observed earlier the kernel K is the normal velocity on the reference helical surface induced by a system of loaded lines emanating from each blade. If the observer is very close to the loaded line on the reference surface, the influence of the other blades will be negligible. Moreover the effect of curvature will be small if the distance from the line to the observer is small compared to the radius of curvature of the helix. Hence the local effect should be essentially the same as that of a straight loaded line on the tangent plane. Thus we shall use a modified form of the planar wing kernel function.

Let $M_o = [U^2+(\Omega r_o)^2]^{1/2}/a_o$ be the helical Mach number at radius r. The form of K_o depends on whether M_o is greater or less than one:

$$K_o(\Delta\bar{\theta},\bar{r},\bar{r}_o) = \frac{C}{\bar{r}_o Y^2}\ \{X + [X^2+BY^2]\}\ \text{sup half}\quad \text{if } M_o < 1$$

$$= \frac{2CH(X)}{\bar{r}_o Y^2}\ [X^2+BY^2]^{1/2}\quad \text{if } M_o > 1 \tag{37}$$

where

$$B = 1 - M_o^2$$

$$C = \frac{M_x}{M_o S^2}\ (1 + (\frac{M_x}{M_o})^2\ \alpha^2)\cdot \frac{1}{\bar{r}} \tag{38}$$

and H is the unit step function, and α is the helical surface curvature at radius $\bar{r}$ defined by Eq. (6).

If we interpret X as being distance downstream and Y perpendicular to a uniform flow at Mach number M_o, then these are the planar wing kernel functions for steady subsonic and supersonic conditions respectively (the supersonic kernel is taken to be zero outside the Mach cone).

In terms of propeller coordinates we take

$$X = \Delta\bar{\theta} + (M_x/M_o)^2\ \alpha(\Delta\bar{r}/\bar{r})$$

$$Y^2 = (M_t/M_o)^2\ [1 + (M_x/M_o)^2\alpha^2](\Delta\bar{r})^2 \tag{39}$$

$$\Delta\bar{r} = \bar{r} - \bar{r}_o$$

It should be noted that the precise form of K_o is rather arbitrary. The only requirement is that K_o should capture the dominant singularity of K and be integrable analytically. The present choice has these properties, though there may well be better choices available.

The corresponding values of D_o can readily be evaluated by use of the following identities. Let $\Delta\bar{\theta}$ be linearly interpolated along the panel edge so that $X = X_o + X'Y$ where X_o and X' are interpolation coefficients determined from the panel edge end points. Let $R(Y) = [X^2+(1-M_o^2)Y^2]^{1/2}$. Note that Y is linear in $\bar{r}_o$ so that integrating in $\bar{r}_o$ is equivalent to integrating in Y. Then, if $d^2 \equiv (X')^2+B$:

$$\frac{X+R}{Y^2} = \frac{d}{dY}\left\{-\frac{X+R}{Y} - X' \ln \frac{X+R}{Y^2} + d \ln (X'X+dR+BY)\right\} \tag{40}$$

gives D_o in the subsonic case;

$$\frac{R}{Y^2} = \frac{d}{dY}\left\{-\frac{R}{Y} - X' \ln \frac{X+R}{Y} + d \ln (X'X+BY+dR)\right\} \tag{41}$$

gives D_o in the supersonic case (subsonic edge, $d^2 > 0$); and

$$\frac{R}{Y^2} = \frac{d}{dY}\left\{-\frac{R}{Y} - X' \ln \frac{X+R}{Y} + |d| \sin^{-1}\left(\frac{X'X+BY}{[-BX_o^2]^{1/2}}\right)\right\} \tag{42}$$

gives D_o in the supersonic case (supersonic edge, $d^2 < 0$).

Section 2

RESULTS

(2.1) *Introduction*

The theory outlined in Section 1 of this report has been implemented in a program UPROP3S (unsteady-propeller-3D-single rotation). Representative results based on that program will be described here, with a view toward demonstrating and verifying the program's capabilities.

In outline the cases which will be discussed are:

1. Convergence Study

   The method is shown to converge when the number of panels is increased. A control point location for best convergence rate is identified.

2. Planar Wing

   The method is shown to reproduce known results for isolated planar wings in steady and unsteady flow.

3. Performance Characteristics

   The theory predicts steady state propeller performance characteristics which are in agreement with existing methods.

4. Ten Bladed Fan Study

   The analysis of a 10 bladed fan shows the same qualitative influence of interblade phase angle on the vibratory response loads as 2-D cascade theory.

5. SR3 propeller

   Generalized forces for structural vibration of an advanced turboprop design are presented.

(2.2) *Convergence and Control Point Position*

The lifting surface integral equation, Eq(23), admits an infinite number of solutions. However, only one is physically acceptable - the one which satisfies the Kutta condition, $\Delta p = 0$ at the trailing edge. Since this condition is not clearly imposed in the numerical scheme, the ability of the method to capture the Kutta condition needs to be demonstrated. To be precise, we must ask the question: does the discrete solution converge to the desired solution of the continuous problem as the number of panels is increased?

Numerical experimentation has indicated that the answer to this question is yes - provided that $\epsilon > \frac{1}{2}$ (i.e. as long as the control point is downstream from the panel midpoint). Thus the numerical Kutta condition is simply $\epsilon > \frac{1}{2}$. (This problem is further discussed in Appendix V.)

We illustrate the convergence properties of the method with an oscillating propeller problem:

Purdue model blade (Table 1)

$$N_B = 1,\ S = 1.7,\ M_x = .1,\ \bar{\omega} = 1$$

$$v_n = \Omega r_t (1 + i\bar{\omega}\,\bar{\theta}) \tag{43}$$

A sequence of calculations were performed in which the number of radial panel rows was fixed at 9 and the number of chordwise panels (NXP) and the control point position (ϵ) were varied.

Fig. (4) shows the fluctuating sectional thrust coefficient (real and imaginary parts) at 80% tip radius. For each value of ϵ, results were calculated at NXP = 4, 8 and 12. The data was then fit with a quadratic in 1/NXP, as shown. The zero intercept is a prediction of the limit value.

The important conclusions to be drawn from this plot are:

- The limit values are insensitive to control point position.
- The choice $\epsilon = .85$ gives nearly the same result for all NXP.
- The algorithm is first order (error proportional to 1/NXP.)

Thus the numerical scheme is convergent and the optimal convergence rate is obtained with $\epsilon = .85$. Similar results for the 2D airfoil problem are given in Appendix V.

The in-phase and out-of-phase parts of the chordwise pressure distribution at $\bar{r} = .8$ are shown in Fig. (5) for the $\epsilon = .85$ case. It is clear that the Kutta condition is captured.

Moreover the pressure distribution (as well as the thrust) is insensitive to NXP at this ε, though of course the larger NXP the better defined the distribution.

All other results reported here will be for $\varepsilon = .85$.

(2.3) *Planar Wing*

The propeller analysis can be used to approximate an isolated planar wing either by taking the speed ratio S ($\Omega r_t /U$) to be very small or by taking the blade span to be small compared to the radius of rotation. The results of such a simulation are shown in Figs. (6, 7) with comparisons to Albano and Rodden's doublet lattice method. [9] The case chosen is an aspect ratio 2 rectangular wing at low Mach number, pitching harmonically about midchord. (Simulated so that the variation in flow speed along the span is less than 1%.)

Figure (6) shows the real and imaginary parts of the chordwise load distribution at midspan for a reduced frequency $\omega c/U = 1$. Fig. (7) shows the total lift coefficient per unit amplitude as a function of reduced frequency.

It is apparent from these comparisons that the present analysis does produce the same results as classical linear unsteady wing theory in this limit.

(2.4) *Propeller Performance*

In this section we will discuss the steady state performance characteristics of three propellers, comparing the predictions of the present lifting surface theory, and Sullivan's vortex lattice method [5-8] which is based on linear incompressible (steady) aerodynamics and so should agree with the present theory at low Mach numbers. Any difference between the two theoretical predictions (at low Mach numbers) then, is a consequence of the different discretization methods. In this regard it should be noted that the two theories differ significantly in the way efficiency is calculated: the present scheme uses the leading edge thrust concept while Sullivan [5] uses the Kutta-Joukowski law.

Results will be presented in terms of the conventional performance parameters:

$$\text{AdvanceRatio} : J = \pi/S \tag{44}$$

$$\text{thrust coefficient} : C_T = \text{thrust} \cdot \pi^2/(4\Omega^2 r_t^4) \tag{45}$$

$$\text{power coefficient} : C_p = \text{power} \cdot \pi^3/(4\Omega^3 r_t^5) \tag{46}$$

$$\text{efficiency} : \eta = JC_T/C_p \tag{47}$$

The three configurations studied (all straight bladed propellers), are:

(a) Purdue model (Table 1) , $N_B = 1$

(b) NACA 109622 (Table 2), $N_B = 3$

(c) SR2 (Table 3), $N_B = 8$.

The chord, twist and camber distributions are given in the indicated Tables. ($\Delta\beta$ is the change in blade setting angle from the 3/4 radius station.)

The normal velocity used in the lifting surface calculation is,

$$v_n = U_r \left[\beta - \tan^{-1}\left(\frac{U}{\Omega r}\right) + \frac{C_{L_D}}{4\pi} \ln\left(\frac{\xi}{1-\xi}\right)\right] . \tag{48}$$

where ξ is the distance along the chord line measured from the leading edge, in units of chord. The C_{L_D} term in this expression is based on the camber line of the 16-series airfoils used on the outboard sections of the SR2 blade (the present calculations use the same airfoil at all radii). The value assigned to C_{L_D} is the 'design' lift coefficient of the airfoil at zero angle of attack (the 16 series airfoils being designed to give a flat load distribution according to linear 2D airfoil theory.) The first two blades are uncambered ($C_{L_D} = 0$) and so derive their thrust from twist only. The SR2 blade is cambered and so derives part of its thrust from the camber.

Figure (8) shows the power and efficiency as a function of advance ratio for the Purdue blade operating at low Mach numbers and $\beta_{3/4} = 45.7^{\circ}$. The two methods predict essentially identical efficiencies. The present method gives a power coefficient slightly (around 10%) lower than the vortex lattice method. (The thrust, which is not shown, must also be slightly lower to get the same efficiency).

Figure (9) shows a similar comparison between the present method and vortex lattice theory, for the three bladed NACA 109622 (again at low Mach number). The two results are clearly very close to each other, with the lifting surface theory now slightly lower in terms of efficiency as well as power and thrust.

The general conclusion to be drawn for Figs. (8) and (9) is that for straight bladed propellers operating at low Mach numbers the present theory predicts essentially the same performance characteristics as the vortex lattice method.

In Fig. (10) we compare the power coefficient predicted by the present scheme to measured values for the SR2 propeller. Three configurations are shown: $(M_x, \beta_{3/4}) = (.3, 40^{\circ})$, $(.3, 52^{\circ})$ and $(.7, 58^{\circ})$. In each case the relative tip Mach number at the lowest advance ratio is near 1. Thus compressibility effects are to be expected. For each blade setting two theoretical predictions are shown - one at low Mach number and one at the experimental value. As would be expected, the incompressible result is low. The predictions using the appropriate Mach number are in very good agreement with experiments.

This indicates that the linear compressibility effects included in the present theory are a significant factor.

(2.5) *Torsional Response of a 10 Bladed Fan*

In this example we consider a fan with 10 blades, each executing a torsional oscillation. The objective of the study is to validate the present theory with regard to the dependence of vibratory response on interblade phase angle.

The blade planform geometry is given in Table 1. The blades are unswept, constant chord, and helically twisted. The operating conditions are defined by M_x=0.1, S = 1.597, $\bar{\omega}$ = 1.0.

The normal velocity distribution on the reference blade is,

$$v_n = U_{rel} \cdot \alpha(1+i\bar{\omega}\,\bar{\theta}) \tag{49}$$

where U_{rel} is the helical velocity and α is the local angle of attack amplitude, which is assumed to vary linearly from hub to tip $\alpha = \bar{r} - \bar{r}_h$.

The aerodynamic response, shown in Figs. (11,12), is measured by the sectional lift coefficient $l/\pi\rho b^3\omega^2$, where b is the blade semi-chord (.23 r_t,) and l is the lift per unit span. Results from Smith's two dimensional cascade theory [10] are included for comparison.

The two figures are for two radii: one inboard, $\bar{r}$ = .6 and one near the tip, $\bar{r}$ = .9. In both cases the 2 and 3 dimensional theories show the same qualitative dependence of load on interblade phase angle. Not surprisingly, the agreement is quantitatively better away from the tip. The 2-D analysis drastically over predicts the inphase loads at $\bar{r}$ = .9 for most interblade phase angles. This is to be expected for an unducted fan and is one of the reasons why a 3-D analysis is preferable.

(2.6) *Generalized Forces for the SR3*

In an aeroelastic calculation the aerodynamic loads induced by blade vibration appear as generalized forces,

$$Q_{jk} = \iint \Delta p_k \, \delta_j \, dA \tag{50}$$

where δ_j is the normal displacement amplitude for the j^{th} mode and Δp_k is the amplitude of the pressure difference across the blade resulting from motion in the k^{th} mode. The vibration is assumed to be simple harmonic with frequency ω.

Generalized force results will be presented here for the SR3CX2, a swept, flexible, advanced turboprop blade designed for flutter testing. In-vacuum vibration mode shapes (including the effects of centrifugal stiffening) were obtained from MSC NASTRAN for 6100 RPM rotational speed with $\beta_{3/4} = 60.7°$. These results were provided to the author by NASA Lewis Research Center.

The normal displacements in mode one are shown in Fig. (13). The generalized force Q_{11} is shown in Fig. (14) as a function of frequency.

References

[1] C.E. Hammond, H.L. Runyan and J.P. Mason, "Application of Unsteady Lifting Surface Theory to Propellers in Forward Flight," AIAA Paper No. 74-419.

[2] D.B. Hanson, "Compressible Helicoidal Surface Theory for Propeller Aerodynamics and Noise," AIAA Journal, Vol. 21, No. 6, June 1983, p. 881.

[3] Farassat, F., "Linear Acoustic Formulas for Calculation of Rotating Blade Noise," AIAA Journal, V. 119, No. 9, Sept. 1981.

[4] Long, L.N., "An Aerodynamic Theory based on Time-Domain Aeroacoustics," AIAA Journal, Vol. 23, No. 6, June 1985.

[5] Sullivan, J.P., Chang, L.K., and Miller, C.J., "The Effect of Proplets and Bi-Blades on the Performance and Noise of Propellers," SAE paper 810600, Apr. 1981.

[6] Chang, L.K., "The Theoretical Performance of High Efficiency Propellers," Ph.D. Thesis, Purdue University, Dec. 1980.

[7] Lesieutre, D.J., and Sullivan, J.P., "The Analysis of Counter Rotating Propeller Systems," SAE Tech. Paper 850869, April 16, 1985.

[8] Mikkelson, D.C., Mitchell, G.A., and Bober, L.J., "Summary of Recent NASA Propeller Research," NASA TM 83733, 1984.

[9] E. Albano and W.P. Rodden, "A Doublet Lattice Method for Calculating Lift Distribution on Oscillating Surfaces in Subsonic Flows," AIAA Journal, Vol. 7, No. 2, Feb. 1969, pp. 279-285.

[10] S.N. Smith, "Discrete Frequency Sound Generation in Axial Flow Turbomachinery," ARC R & M 3709, 1973.

[11] Lowson, M.V., "The sound field for singularities in motion," Proceedings of the Royal Society (London), Volume A286, 1985, pp, 559-572.

[12] Sears, W.R. (ed), "General Theory of High Speed Aerodynamics" vol VI of "High Speed Aerodynamics and Jet Propulsion" Princeton University Press, Princeton N.J., 1964

[13] Williams, M.H., 'An Unsteady Lifting Surface Theory for Single Rotation Propellers', Purdue University Report, School of Aeronautics and Astronautics,

June, 1985

[14] Williams, M.H., 'User's Guide to UPROP3S', Purdue University Report, School of Aeronautics and Astronautics, January, 1985

Appendix I
Velocity Induced by a Moving Point Force

Consider a uniform unbounded stationary fluid with density ρ_o and sound speed a_o. We imagine that this fluid is disturbed by the action of a point force moving along some prescribed path. The resulting pressure disturbance, p', and velocity, $\vec{u}$, are presumed to obey the linear acoustic equations of continuity and momentum conservation:

$$\frac{\partial p'}{\partial t} + \rho_o a_o^2 \, \nabla\cdot\vec{u} = 0 \tag{I.1}$$

$$\rho_o \frac{\partial \vec{u}}{\partial t} + \nabla p' = \vec{F}(t)\, \delta(\vec{x}-\vec{x}_o(t)) \tag{I.2}$$

where $-\vec{F}$ is the force exerted on the fluid and $\vec{x}_o$ is its point of application.

The solution of these equations for p' has been given by Lowson [11]. In this application, though, we need the velocity. To get it we introduce a "displacement potential," ψ (such that $\nabla\psi$ is the particle displacement):

$$\vec{u} = \frac{\partial}{\partial t} \nabla\psi + \vec{u}_\delta \tag{I.3}$$

$$p' = -\rho_o \frac{\partial^2 \psi}{\partial t^2}\,, \tag{I.4}$$

where $\vec{u}_\delta$ is an impulsive velocity concentrated on the trajectory. Substituting these definitions into the momentum equation, Eq(I.2) yields an expression for $\vec{u}_\delta$.

$$\frac{\partial \vec{u}_\delta}{\partial t} = \frac{1}{\rho_o} \vec{F}(t)\, \delta(\vec{x}-\vec{x}_o(t)) \tag{I.5}$$

while, from the continuity relation (I.1) we get:

$$\frac{\partial}{\partial t} [\nabla^2\psi - \frac{1}{a_o^2} \frac{\partial^2 \psi}{\partial t^2}] = \nabla.\vec{u}_\delta \tag{I.6}$$

Integrating (I.5 and I.6) over time yields:

$$\vec{u}_\delta = \frac{1}{\rho_o} \int_{-\infty}^{\infty} \vec{F}(t_1)\, \delta(\vec{x}-\vec{x}_o(t_1))H(t-t_1)dt_1 \tag{I.7}$$

$$\nabla^2\psi - \frac{1}{a_o^2} \frac{\partial^2 \psi}{\partial t^2} = \frac{1}{\rho_o} \nabla. \int_{-\infty}^{\infty} \vec{F}(t_1)\delta(\vec{x}-\vec{x}_o(t_1))(t-t_1)H(t-t_1)dt_1 \tag{I.8}$$

where H is a Heaviside step function.

Note that $\vec{u}_\delta$ vanishes everywhere except on the trajectory of the point force.

The solution of (I.8) for the displacement potential can be obtained from the point source solution to the wave equation:

$$(\nabla^2 - \frac{1}{a_o^2}\frac{\partial}{\partial t^2})\{\frac{f(t-t_1-R_1/a_o)}{4\pi R_1}\} = -\delta(\vec{x}-\vec{x}_o(t_1))f(t-t_1) \tag{I.9}$$

where $R_1 = |\vec{x}-\vec{x}_o(t_1)|$ and f(t) is an arbitrary function. From this it is apparent that ψ is given by:

$$\psi = -\frac{1}{4\pi\rho_o}\nabla\cdot\int_{-\infty}^{\infty}\vec{F}(t_1)\frac{(t-t_1-R_1/a_o)H(t-t_1-R_1/a_o)}{R_1}dt_1 \tag{I.10}$$

After performing the divergence operation we get,

$$\psi = \frac{1}{4\pi\rho_o}\int_{-\infty}^{\infty}\frac{\vec{F}_1\cdot\vec{R}_1}{R_1^3}(t-t_1)H(t-t_1-R_1/a_o)dt_1 \tag{I.11}$$

The step function in the integrand means that we need integrate only over that part of the trajectory which is acoustically accessible to the field point. We may remove the step function by introducing the retarded time τ, which is the time at which a sound wave must be emitted from the source in order to arrive at the field point $\vec{x}$ at time t. For fixed field point position and time, the retarded time must be determined by finding the roots of the transcendental equation,

$$t = \tau + R(\tau)/a_o\ . \tag{I.12}$$

Differentiating this relation with respect to τ yields

$$\frac{dt}{d\tau} = 1 - \frac{\vec{u}_o}{a_o}\cdot\frac{\vec{R}}{R} = 1-M_R \tag{I.13}$$

where $\vec{u}_o = \dot{\vec{x}}_o(\tau)$ is the velocity and M_R is the Mach number in the direction of the observer. Clearly if the force moves subsonically then there can be only one τ for each t (since M_R is then everywhere less than one). If the source Mach number is greater than one, though, there may be several retarded times (or none) which satisfy Eq(I.12).

In general, let τ_1, τ_2, τ_3 ... etc. be the ordered roots of (I.12). Let us further assume that $M_R < 1$ at τ_1. Then we must have $M_R > 1$ at τ_2, $M_R < 1$ at τ_3 etc., since the extrema ($M_R = 1$ or $\frac{dt}{d\tau} = 0$) must occur in between roots. It follows that for any function f(t):

$$\int_{-\infty}^{\infty} f(t_1)H(t-t_1-R_1/a_o)dt_1 = \int_{-\infty}^{\tau_1} f(t_1)dt_1 + \int_{\tau_2}^{\tau_3} f(t_1)dt_1 + \int_{\tau_4}^{\tau_5} f(t_1)dt_1 + \cdots$$

$$= \int_{-\infty}^{\tau_1} f(t_1)dt_1 - \int_{-\infty}^{\tau_2} f(t_1)dt_1 + \int_{-\infty}^{\tau_3} f(t_1)dt_1 - \cdots$$

$$= \sum_{\tau} \frac{1-M_R}{|1-M_R|} \int_{-\infty}^{\tau} f(t_1)dt_1 \qquad (I.14)$$

where M_R is evaluated at the root τ and the summation is over all possible roots.

The result (I.11) for the displacement potential can thus be expressed as:

$$\psi = \frac{1}{4\pi\rho_o} \sum_{\tau} \frac{1-M_R}{|1-M_R|} \int_{-\infty}^{\tau} (t-t_1) \frac{\vec{F}_1 \cdot \vec{R}_1}{R_1^3} dt_1 \ . \qquad (I.15)$$

To get the particle displacement we need the result (from (I.12)) that

$$\nabla\tau = -\frac{\vec{N}}{a_o(1-M_R)} \qquad (I.16)$$

$$\vec{N} = \vec{R}/R$$

where $\vec{N}$ is a unit vector directed from the source at $\vec{x}_o(\tau)$ to the observer.

It follows directly that the velocity is

$$\vec{u} = \frac{\partial}{\partial t} \left[\frac{1}{4\pi\rho_o} \sum_{\tau} \frac{1-M_R}{|1-M_R|} \vec{G}(\tau) \right] \qquad (I.17)$$

where

$$\vec{G}(\tau) = -\frac{\vec{N}(\vec{F}\cdot\vec{N})}{a_o^2 R(1-M_R)} + \int_{-\infty}^{\tau} \frac{t-t_1}{R_1^3} [\vec{F}_1 - 3\vec{N}_1(\vec{F}_1 \cdot \vec{N}_1)]dt_1 \qquad (I.18)$$

Note that $\vec{G}$ (and therefore $\vec{u}$) is infinite on the trajectory (since $R_1 = 0$ on the path of integration), and, in the supersonic case, on the Mach cone $M_R = 1$.

Equations (I.17-18) give the fluid velocity induced by a varying point force moving along an arbitrary path.

Appendix II
Kernel Function for Helical Lifting Surfaces

The results of Appendix I are for an arbitrary time dependent force moving along an arbitrary path. We now specialize to the case of helical motion and a harmonically fluctuating force. The path of the force, is, then,

$$x_o(t) = \bar{x}_o - Ut\ ,\ \ \theta_o(t) = \bar{\theta}_o - \Omega t,\ r_o = \text{const.}\ . \tag{II.1}$$

The force, $\vec{F}$ is perpendicular to the helical surface at $\vec{x}_o$, so if $\Delta p(r_o, \bar{\theta}_o)$ is the amplitude of the pressure difference across the surface, then

$$\vec{F}(t) = f\vec{L}_o\, e^{i\omega t}$$

where,

$$f \equiv \Delta p(r_o, \bar{\theta}_o)\, r_o dr_o d\bar{\theta}_o \tag{II.2}$$

$$\vec{L}_o = \vec{L}(\vec{x}_o(t))$$

($\vec{L}$ is the surface normal defined in Eq. (5).)

Now let $\vec{L} = \vec{L}(\vec{x})$ be the normal to the helical surface at the field point $\vec{x}$. From Eq.'s (I.17,18) and (II.2), the induced normal velocity is

$$\vec{u}\cdot\vec{L} = \frac{f}{4\pi\rho_o}\,\frac{\partial}{\partial t}\,\{\sum_{\tau}\,\frac{1-M_R}{|1-M_R|}\,G\} \tag{II.3}$$

where

$$G = -\,\frac{(LN)(L_oN)}{a_o^2R(1-M_R)}e^{i\omega\tau} + \int_{-\infty}^{\tau}\,\frac{t-t_1}{R_1^3}\,e^{i\omega t_1}\,[LL-3LN\cdot L_oN]_1\,dt_1 \tag{II.4}$$

and where,

$$LN = \vec{L}\cdot\vec{N} = \vec{L}\cdot\vec{R}/R$$

$$L_oN = \vec{L}_o\cdot\vec{N} \tag{II.5}$$

$$LL \equiv \vec{L}_o\cdot\vec{L}\ .$$

Explicit expressions for the geometric quantities R, LN, etc. will be given below. In Eqs. (II.3,4) all variables subscripted "1" are evaluated at the dummy time t_1; unsubscripted variables are evaluated at the retarded time τ.

Given (II.1), time can clearly be replaced by the force's position. Thus let,

$$\gamma_1 \equiv \theta - \theta_o(t_1)$$

$$\gamma \equiv \theta - \theta_o(\tau) \tag{II.6}$$

$$\Omega t = \bar{\theta} - \theta \, .$$

With these substitutions (t_1 by γ_1, τ by γ, and t by $\bar{\theta}$), Eq. (II.4) becomes

$$G = \frac{\Omega}{U^3} e^{i\bar{\omega}(\bar{\theta}_o - \theta)} \bar{G}(\gamma) \tag{II.7}$$

$$\bar{G}(\gamma) = - \frac{M_x^2 \, LN \, L_o N}{\hat{R}(1 - M_R)} \, e^{i\bar{\omega}\gamma} \tag{II.8}$$

$$+ \int_{-\infty}^{\gamma} \frac{(\Delta\bar{\theta} - \gamma_1)}{\hat{R}_1^3} \, e^{i\bar{\omega}\gamma_1} \, [LL - 3LN \cdot L_o N]_1 \, d\gamma_1$$

$$\bar{\omega} = \omega/\Omega$$

$$\hat{R} \equiv \Omega R/U$$

$$\Delta\bar{\theta} = \bar{\theta} - \bar{\theta}_o \, ,$$

Note that the retarded time relation becomes a retarded angle equation,

$$\Delta\bar{\theta} = \gamma + M_x \hat{R} \tag{II.9}$$

Substituting Eq (II.7) into Eq. (II.3) we get

$$4\pi \vec{u} \cdot \vec{L} e^{i\bar{\omega}\theta} = \frac{\Omega f}{\rho_o U^3} \, e^{i\bar{\omega}\bar{\theta}_o} \, \frac{\partial}{\partial t} \left\{ \sum_{\gamma} \frac{1 - M_R}{|1 - M_R|} \, \bar{G}(\gamma) \right\} \tag{II.10}$$

Because the right hand side of this expression depends on time only through $\bar{\theta} = \theta + \Omega t$, the time derivative can be replaced by an angle derivative ($\frac{\partial}{\partial t} = \Omega \frac{\partial}{\partial \bar{\theta}}$). Thus (reintroducing the pressure difference Δp) we obtain:

$$4\pi (\vec{u} \cdot \vec{L}) e^{i\bar{\omega}\bar{\theta}} = \frac{\Omega^2 \Delta p}{\rho_o U^3} \, e^{i\bar{\omega}\bar{\theta}_o} \, \frac{\partial}{\partial \bar{\theta}} \, \bar{K}(\bar{\theta} - \bar{\theta}_o, \, r_o, \, r) d\bar{\theta}_o \, r_o dr_o \tag{II.11}$$

where

$$\bar{K} = \sum_{\gamma} \frac{1-M_R}{|1-M_R|} \bar{G} . \qquad \text{(II.12)}$$

Multiple Blades

This gives the normal velocity induced by a single point force on one blade. If there are multiple (N_B) blades, let them be counted j = 1, ..., N_B counterclockwise, so that

$$(\bar{\theta}_o)_j = (\bar{\theta}_o)_1 + (j-1)\Delta\theta_B \ , \ \Delta\theta_B = 2\pi/N_B \ , \qquad \text{(II.13)}$$

are the angular positions of all blade points at the same r_o, $\bar{x}_o$. Suppose, further, that the loads are periodic from blade to blade,

$$(\Delta p)_j = (\Delta p)_1 \ e^{im(j-1)\Delta\theta_B} \qquad \text{(II.14)}$$

Then the net velocity induced by all N_B points is given by Eq. (II.11) if $\bar{K}$ is replaced therein by

$$K(\bar{\theta}-\bar{\theta}_{o1}, r_o, r) = \sum_{j=1}^{N_B} e^{i(\bar{\omega}+m)\Delta\theta_B(j-1)} \bar{K}(\bar{\theta}-\bar{\theta}_{oj}, r_o, r) \qquad \text{(II.15)}$$

Geometric Relations

For the sake of completeness we list here various purely geometric and kinematic relations.

- $$\Delta x = x - x_o(\tau) = \frac{U}{\Omega} (\gamma + \Delta\sigma) \qquad \text{(II.16)}$$

  where $\Delta\sigma = \sigma - \sigma_o$.

- $$\hat{R} = \Omega R/U \qquad \text{(II.17)}$$

  where $R^2 = (\Delta x)^2 + r^2 + r_o^2 - 2rr_o \cos\gamma$

- $$LN = \bar{L}\cdot\bar{N} \qquad \text{(II.18)}$$

$$= [\gamma + \Delta\sigma - \frac{r_o}{r}(\sin\gamma - \alpha\cos\gamma) - \alpha]/\hat{R}$$

- $$L_o N = \bar{L}_o \cdot \bar{N} \tag{II.20}$$

$$= [\gamma + \Delta\sigma - \frac{r}{r_o}(\alpha_o \cos\gamma + \sin\gamma) + \alpha_o]/\hat{R}$$

- $$LL = \bar{L}_o \cdot \bar{L} \tag{II.21}$$

$$= 1 + \frac{U^2}{\Omega^2 r r_o}[(1+\alpha\alpha_o)\cos\gamma + (\alpha - \alpha_o)\sin\gamma]$$

- $$\alpha = r\sigma'(r),\ \alpha_o = r_o\sigma'(r_o) \tag{II.22}$$

- $$M_R = \bar{M}_o \cdot \bar{N} \tag{II.23}$$

$$= -M_x[\gamma + \Delta\sigma + \frac{\Omega^2 r r_o}{U^2}\sin\gamma]/\hat{R}$$

Summary

The collective kernel function for N_B blades with interblade phase index m is given by Eq. (II.15). The single blade kernel is obtained from Eq. (II.12) and (II.8).

Appendix III

Numerical Evaluation of the Kernel Function

The kernel function K, defined by Eqs. (II.8), 12, 15, must be evaluated for specified radii (r, r_o) over a range of angular separations $\Delta\bar{\theta}_{max} > \Delta\bar{\theta} > \Delta\bar{\theta}_{min}$. (The range is determined by the blade planform at radii r and r_o). In the procedure described here the function $K(\Delta\bar{\theta})$ (for fixed r and r_o) is defined numerically by constructing a table K_J, $\Delta\bar{\theta}_J$, $J = 1, N_K$, which spans the required domain of $\Delta\bar{\theta}$. Values of K for specific combinations of control and load point can then be found by interpolation.

In the first step, the function $\bar{G}(\gamma)$, defined by Eq. (II.8), is split into:

$$\bar{G} = \bar{G}_o(\gamma) + \Delta\bar{\theta}(B_o(\gamma) - B_o(-\infty)) - B_1(\gamma) \tag{III.1}$$

where

$$G_o(\gamma) = -\frac{M_x^2(LN)(L_oN)}{\hat{R}(1-M_R)}\, e^{i\bar{\omega}\gamma} \tag{III.2}$$

is the algebraic part of $\bar{G}$, and:

$$B_o(\gamma) = \int_{\gamma max}^{\gamma} b(\gamma_1)/\hat{R}_1^3 d\gamma_1 \tag{III.3}$$

$$B_1(\gamma) = \int_{\gamma max}^{\gamma} \gamma_1 b(\gamma_1)/\hat{R}_1^3 d\gamma_1 \tag{III.4}$$

$$b(\gamma) = e^{i\bar{\omega}\gamma}[LL-3(LN)(L_oN)] \,. \tag{III.5}$$

Note that γmax is an arbitrary constant and that the additive constant $B_1(-\infty)$ has been deleted from Eq. (III.1) (which is allowed by the fact that only changes in $\bar{G}$ are physically significant).

For the reference blade the computation is begun by choosing γmax such that the corresponding $\Delta\bar{\theta}$ (given by Eq. (II.9)) is just larger than the largest required value, $\Delta\theta max$. The calculation is then marched backward in constant increments $\Delta\gamma$ from γmax. At each step the corresponding value of $\Delta\bar{\theta}$ and a provisional value of $\bar{G}$ (without the $B_o(-\infty)$ term) are computed and saved in arrays. In addition the current value of B_o is retained (so that $B_o(-\infty)$ may eventually be found.) This procedure is terminated when $\Delta\bar{\theta}$ becomes less than the minimum required value.

At this point the B_o integration is continued (generally with a larger $\Delta\gamma$) until the sending point is a prescribed axial distance downstream (*eg* five tip radii.) The final

value of B_o is taken as $B_o(-\infty)$ and the correction term $\Delta\bar{\theta}\, B_o(-\infty)$ is subtracted from each element of the $\bar{G}$ vector. The vectors $\Delta\bar{\theta}$ and $\bar{G}$ then contain, in tabular form, the information needed to define the influence of any point at radius r_o on any point at r for a given blade.

If r_o is subsonic then $\bar{G}$ is identical to the single blade kernel $\bar{K}$ (cf Eq. (II.12)). However, if r_o is supersonic then $\Delta\bar{\theta}$ is a non-monotonic function of γ (with extrema at $M_R = 1$) and the tables $\Delta\bar{\theta}$ and $\bar{G}$ must be interpolated onto new arrays giving $\bar{K}$ at an ordered sequence of $\Delta\bar{\theta}$.

Having found $\bar{K}$ for the reference blade, the entire procedure is then repeated for each subsequent blade. However, the elements of the $\Delta\bar{\theta}$ vector are not the same as those for the reference blade. Hence for all subsequent blades the tables $\bar{K}$, $\Delta\bar{\theta}$ must be interpolated onto the table for the reference blade.

After the calculation has been completed for all blades, one has N_B+1 vectors: $\Delta\bar{\theta}$ and $\bar{K}$ for each blade. The kernel functions are then added with appropriate phasing to form the collective kernel, according to Eq. (II.15).

Numerical Integration Method

In this section the numerical method used to evaluate the integrals B_o and B_1, defined in Eqs. (III.3-III.5), are described.

Note that the integrands contain only algebraic and trigonometric functions of the dummy variable γ_1. By integrating in equal increments, $\Delta\gamma$, the required trigonometric functions can be generated recursively at each step (with some gain in computational efficiency).

A simple quadrature, like Simpson's rule, cannot be used, however, because the denominator, $\hat{R}_1^3$, may assume very small values over part of the integration range (when the control point is close to the loaded line). In order to circumvent this difficulty we use the rule:

$$\int_{\gamma_1}^{\gamma_2} \frac{u(\gamma)}{R^3(\gamma)}\, d\gamma = \frac{2\Delta\gamma}{(R_1+R_2)^2-c}\left(\frac{u_2}{R_2}+\frac{u_1}{R_1}\right) \tag{III.6}$$

which is exact if the numerator, $u(\gamma)$, is linear and $R^2(\gamma)$ is quadratic,

$$R^2(\gamma) = a + b\varepsilon + c\varepsilon^2,\ \varepsilon = (\gamma-\gamma_1)/\Delta\gamma \tag{III.7}$$

between the limits of integration. Note that the constant and linear coefficients , a and b, are not needed in Eq.(III.7), but the quadratic coefficient, c, is. An expression for c will be worked out below.

Since $\hat{R}^2$ is not quadratic, but involves a cosine of the retarded angle, the constant c must be determined by a curve fit. For this purpose we introduce the quadratic interpolation,

$$\cos\gamma = (1-\epsilon^2)\cos\gamma_1 + \epsilon^2\cos\gamma_2 + B\,\epsilon(1-\epsilon) \tag{III.8}$$

$$\epsilon = (\gamma-\gamma_1)/\Delta\gamma, \text{ in } [0,1]$$

$$B = -\Delta\gamma[1 + (\Delta\gamma)^2/12]\sin\gamma_1 .$$

(The maximum error over the interval involved in this expression is $(\Delta\gamma)^3 \sin\gamma_1/72\sqrt{3}$.)

The exact expression for $\hat{R}^2$ is (cf Eqs. (II.12,13))

$$\hat{R}^2 = (\gamma+\Delta\sigma)^2 + D_o - D_1\cos\gamma \tag{III.9}$$

where D_o, D_1 and $\Delta\sigma$ depend only on radius.

Inserting Eq. (III.8) into (III.9) yields the constant c required in Eq. (III.6):

$$c = (\Delta\gamma)^2 - D_1[\cos\gamma_2 - \cos\gamma_1 + \Delta\gamma(1 + \frac{(\Delta\gamma)^2}{12})\sin\gamma_1] \tag{III.10}$$

Note that c is small and so has an effect on the integral only if R_1 and R_2 are themselves small.

Formulas III.6 and III.10, together with a recursive evaluation of sin and cos, constitute the algorithm for computing B_o and B_1.

Appendix IV

Efficiency Calculation

The steady state efficiency of a propeller is the ratio of the work done in forward motion to that done in rotation,

$$\eta = \frac{UT}{UT+P_L} \tag{IV.1}$$

where P_L is the power loss from induced and viscous drag ($(UT+P_L)/\Omega$ is the shaft torque). Neglecting viscous losses, P_L is the rate of work done by the pressure forces acting over the blade,

$$P_L = -\iint p\vec{n}\cdot\vec{u}dA\ . \tag{IV.2}$$

Note that P_L is quadratic in the disturbances while UT is linear (so η will generally be close to unity). In linear aerodynamic theory the errors in thrust (resulting from the linearization) are quadratic and therefore comparable to P_L. The efficiency can be computed using linear theory only because η depends on the ratio P_L/UT, which is linear.

In linear theory the blade is represented by a helical sheet on which there is a load Δp and a prescribed normal velocity. Part of the power loss, then, comes from the distributed loads on the sheet,

$$P_{LS} = -\iint \Delta p\ \vec{L}\cdot\vec{u}\ r\ dr\ d\bar{\theta} \tag{IV.3}$$

where $\vec{L}$ is the normal to the helical surface. This part can be computed quite simply once the load distribution has been found.

In addition to the distributed loads on the surface, however, there are concentrated forces acting at the leading edge, caused by the locally infinite velocities and pressures. These forces are quadratic in the disturbances levels and so contribute negligibly to the overall forces on the blade. However they act generally in the direction of motion (rather than at the right angles at it, like the surface forces) and so produce a contribution to the power which is comparable to P_{LS}.

Let $\vec{U}$ be the blade velocity and $d\vec{F}_L$ an incremental leading edge force. The net power loss generated, then, is

$$P_{LL} = -\int_{LE} \vec{U}\cdot d\vec{F}_L\ . \tag{IV.4}$$

Our object here is to relate this quantity to the computed load distribution, Δp, and the

leading edge geometry.

Let $s_L(r)$ be the arclength along, and $\vec{n}_L(r)$ the unit vector normal to the leading edge at radius r (we take $\vec{n}_L$ to be on the helical surface and directed away from the blade). From a momentum balance in the locally two dimensional flow in the plane perpendicular to the leading edge, we find that the force on an increment of length ds_L is:

$$d\vec{F}_L = \pi\rho\beta_L K_v^2 \vec{n}_L ds_L \tag{IV.5}$$

where

$$\beta_L = [1-(\vec{U}\cdot\vec{n}_L/a_o)^2]^{1/2} \tag{IV.6}$$

is the normal Prandtl-Glauert parameter. The factor K_v measures the strength of the leading edge velocity singularity. Let μ be the distance from the leading edge measured inboard along the local normal $\vec{n}_L$. Then, if $u_L(\mu)$ is the velocity in the normal direction,

$$K_v = \lim_{\mu\to o} (u_L\sqrt{\mu}) . \tag{IV.7}$$

Note that the force $d\vec{F}_L$ is in the direction of motion so that P_{LL} is negative (i.e. the leading edge forces act like a power source).

The above expression for the leading edge force is a simple restatement of Eqs. (9.15) and (9.16) in Ref.[12]. To be useful, though, the coefficient K_v must be calculated from Δp.

Let ξ be the distance measured inboard from the leading edge in the $\vec{U}$ direction and let Λ be the angle between $\vec{n}_L$ and $\vec{U}$ (i.e. Λ is the leading edge sweep angle). Referring to Fig. (1) we see that $\mu = \xi \cos\Lambda$.

Define a pressure coefficient singularity strength K_p by

$$K_p = \lim_{\xi\to o} [-\sqrt{\xi}\,\frac{\Delta p}{\rho|\vec{U}|^2}] . \tag{IV.8}$$

From Bernoulli's equation, then, the velocity potential behaves like

$$\phi \to |\vec{U}|\, K_p \sqrt{\xi} . \tag{IV.9}$$

Therefore, from Eqs. (IV.8) and (IV.9),

$$K_v = \lim \sqrt{\mu}\,\frac{\partial\phi}{\partial\mu} = \frac{1}{2}\,|\vec{U}|K_p/\sqrt{\cos\Lambda} . \tag{IV.10}$$

Finally, since $\vec{U}\cdot\vec{n}_L = |\vec{U}|\cos\Lambda$, we obtain the incremental power in the form, (from Eq. (IV.5) and (IV.10))

$$\vec{U}\cdot d\vec{F}_L = \frac{\pi}{4}\rho\beta_L |\vec{U}|^3 K_p^2 \, ds_L \, . \qquad \text{(IV.11)}$$

This expression is convenient when (as here) the load Δp is computed in strips running parallel to $\vec{U}$.

Finally we give some useful geometric results for the propeller. Recall that the helical surface is on $\bar{x} = U/\Omega\,(\bar{\theta} + \sigma(r))$. Let $\bar{\theta}_L$ and $\bar{x}_L$ be the leading edge coordinates. Define

$$\gamma_L = r\frac{d\bar{\theta}_L}{dr} \qquad \text{(IV.12)}$$

$$S_r = \Omega\, r/U \, .$$

Then

$$\frac{ds_L}{dr} = [1 + (\gamma_L+\alpha)^2/S_r^2 + \gamma_L^2]^{1/2} \qquad \text{(IV.13)}$$

defines distance along the leading edge, and

$$\xi = \frac{|\vec{U}|}{\Omega}(\bar{\theta}-\bar{\theta}_L) \qquad \text{(IV.14)}$$

defines distance inboard from the leading edge (recall that $\alpha = r d\sigma/dr$, as previously defined).

The component of velocity normal to the leading edge is given by

$$(\vec{U}\cdot\vec{n}_L)^2 = (|\vec{U}|^2 + \alpha^2U^2)(\frac{ds_L}{dr})^{-2} \qquad \text{(IV.15)}$$

(which can most readily be shown by first evaluating the component along the edge).

Finally we give the two power losses in terms of the nondimensional load, $P = S^2\Delta p/\rho U^2$ and nondimensional normal velocity $W = 4\pi\vec{L}\cdot\vec{u}/U$, which are the variables used in the lifting surface integral equation.

$$\frac{P_{LS}}{\rho\Omega^2 r_t^4 U} = -\frac{1}{4\pi S^4}\int_0^1\!\!\int PW d\bar{\theta}\bar{r}d\bar{r} \qquad \text{(IV.16)}$$

$$\frac{P_{LL}}{\rho\Omega^2 r_t^4 U} = -\frac{\pi}{4S^7}\int_0^1 \beta_L C\frac{dS_L}{dr}\,d\bar{r} \qquad \text{(IV.17)}$$

where

$$C = \lim [(\bar{\theta}-\bar{\theta}_L)P^2]$$

$$\beta_L^2 = 1 - M_x^2(1 + \alpha^2 + \bar{r}^2 S^2)/(\frac{dS_L}{dr})^2 . \qquad \text{(IV.18)}$$

The total inviscid power loss is $P_L = P_{LL} + P_{LS}$.

In order to implement this scheme for computing efficiency the leading edge singularity strength C must be extracted from the numerical data. Let P_1 be the value of P on the leading edge panel, which has a length $\Delta\bar{\theta}_1$. The associated force is $P_1\Delta\bar{\theta}_1$. The same net force is produced by the variable load

$$P = \frac{1}{2} P_1 [(\Delta\bar{\theta}_1) / (\bar{\theta}-\bar{\theta}_L)]^{.5} , \qquad \text{(IV.19)}$$

which implies a leading edge strength

$$C = \frac{1}{4} P_1^2 \Delta\bar{\theta}_1 . \qquad \text{(IV.20)}$$

Note that this is equivalent to saying that the load P_1 is the load at the 1/4 chord of the first panel. (The same argument would assign the inboard loads to points close to the midchord of each panel.) The accuracy of this numerical method for computing the leading edge singularity strength is discussed in Appendix V. It is shown there that although the panel scheme converges almost everywhere, the leading edge strength has a residual error of about 10% in the limit of increasing panel density. It has been found that increasing C by a factor 1.1 significantly improves the prediction of leading edge suction, and therefore of induced drag.

In summary, the efficiency is computed from Eqs. (IV.1, 12, 13, 16, 17, 18 and 20).

Appendix V

2-D Airfoil Test Case

The constant load panel method was tested on the simple case of a 2-D thin airfoil in steady incompressible flow, for which an exact solution is well known. This test sheds some light on the selection of control point position and the identification of the leading edge singularity strength (which is required to calculate propeller efficiency.)

The vertical velocity v(x) induced by a unit length vortex sheet of strength $\gamma(x)$ is

$$v(x) = \frac{1}{\pi} \int_0^1 \frac{\gamma(\xi)}{x-\xi} \, d\xi \tag{V.1}$$

If, for example, we require that v(x) = 1 for x in (0,1) then the solution which obeys the Kutta condition $\gamma(1) = 0$ is,

$$\gamma(x) = [(1-x) / x]^{.5} \tag{V.2}$$

so that the total circulation and leading edge singularity strength are,

$$\Gamma = \int_0^1 \gamma(x) dx = \frac{\pi}{2} \tag{V.3}$$

$$C = \sqrt{x}\, \gamma(x) \,|_{x=0} = 1 \tag{V.4}$$

We will examine the ability of the constant strength panel method to predict this solution. Using N equal length panels and a control point located a fraction ϵ back from the leading edge of each panel, the corresponding discrete problem is

$$\frac{1}{\pi} \sum_{j=1}^{N} \gamma_j^N \ln \left| \frac{k-j+\epsilon}{k-j+\epsilon-1} \right| = 1 \; ; \; k = 1, N \tag{V.5}$$

$$\Gamma_N = \frac{1}{N} \sum_{j=1}^{N} \gamma_j^N \tag{V.6}$$

For the leading edge singularity we examine two approximations,

$$C_1^N = \gamma_1^N / 2\sqrt{N} \tag{V.7}$$

$$C_2^N = [\gamma_1^N - \frac{1}{\sqrt{8}} (\gamma_1^N + \gamma_2^N)] / \sqrt{N} \, . \tag{V.8}$$

The first of these (which is the direct analogue of Eq. (IV.20)) is obtained from equating the first panel circulation, $\gamma_1^N \Delta x$, to the circulation for the distribution $C/\sqrt{x}$. Eq. (V.8)

is obtained by the same matching for the first two panels with an assumed distribution $C/\sqrt{(x)}\ (1+bx)$.

We first examine the convergence of the scheme with respect to net circulation Γ (global convergence), and the choice of control point.

Note, first, that the solution for N = 1 is, trivially,

$$\Gamma^1 = \gamma_1^1 = \pi / \ln|\varepsilon/(\varepsilon-1)| \tag{V.9}$$

This is singular at $\varepsilon = 1/2$ and antisymmetric in reflection $\varepsilon \rightarrow 1-\varepsilon$. In fact the same thing is true for any value of N - so that the numerical method cannot converge to the desired solution for all ε.

Note, secondly, that $\Gamma^1 = \pi/2$ if $\varepsilon = 1/(1 \pm e^{-2}) = .88$ or 1.16. The region around .88 is examined in detail in Fig. (V.1), which shows the percentage error $2\Gamma_N/\pi - 1$ for a range of N and ε. The error evidently decreases to 0 as N increases for all values of ε shown, indicating that the scheme in fact does converge to the desired solution.

It appears that the scheme will converge (to Eq. (V.2)) for any $\varepsilon > \frac{1}{2}$. For $\varepsilon < \frac{1}{2}$, it must converge to the image solution with Kutta condition at the leading edge. (As noted before the solution is always singular at $\varepsilon = \frac{1}{2}$.)

Again referring to Fig. V.1, it is apparent that for each N there is a point of zero error, which drops from $\varepsilon = .88$ when N = 1 to around .845 when N is large. The choice $\varepsilon = .85$, which was (by a similar study) found to be optimal in the propeller problem, is also optimal here, producing no more than 0.1% errors in Γ if $N \geq 8$.

While the scheme converges globally (whenever $\varepsilon > .5$), it does not appear to converge locally at the leading edge (where the limit solution is infinite.) This is illustrated in Fig. V.2, which shows predictions of C from Eqs. (V.7,8) for $\varepsilon = .85$ and .82. The various curves shown do not approach the correct value (1) at large N, or even a common value. Furthermore, the "second order" fit, Eq. (V.8), is not noticeably more accurate than Eq. (V.7).

Despite the lack of convergence, the results (for C^2) are within 10% of the correct value. This kind of error in leading edge singularity strength implies acceptable accuracy in the prediction of propeller efficiency.

Appendix VI

Aeroelastic Analysis

Although the aeroelastic analysis of the rotor is not strictly the topic of this report, the code in which the method under discussion is implemented contains options for doing both forced response and stability calculations. Therefore the methods used will be described here. The reader who wishes to supply his own aeroelastic analysis and only use the aerodynamic solutions can easily do so.

We assume that the blade deformation is described by a generalized coordinate vector q,of length N_{mode}, with corresponding mass, damping and stiffness matrices M,C and K respectively. The equations of motion of the blade are

$$M\ddot{q} + C\dot{q} + Kq = F(t) \tag{VI.1}$$

where the i'th generalized force F_i is the virtual work done by the aerodynamic load Δp against a unit amplitude deformation in the i'th mode,

$$F_i(t) = \iint \delta_i \Delta p dA \tag{VI.2}$$

In general we can take the force to consist of motion independent and motion dependent parts,

$$F = F_0 + \int_{-\infty}^{t} A(t-\tau)\dot{q}(\tau)\, d\tau \tag{VI.3}$$

where F_0 is the motion independent force and A is the generalized derivative of the force with respect to the modal coordinates (or ,equivalently, the force induced by a unit step in a modal displacement.) Although we cannot easily determine the detailed form of A from the present method, it is important that it depends only on the time lag $t-\tau$ rather than on t and τ separately.

Forced Response

In the forced response case we take F_0 to be simple harmonic with some prescribed frequency ω and interblade phase index m. The solution of Eq. (VI.1) will then have the same structure, so that,

$$F_0 = Re(\bar{F}_0 e^{i\omega t}) \tag{VI.4}$$

$$q = Re(\bar{q} e^{i\omega t}) \tag{VI.5}$$

where the complex amplitudes are related by,

$$\bar{q} = [\, -M\,\omega^2 + i\,\omega\,C + K - Q\,]^{-1}\bar{F}_0 \qquad \text{(VI.6)}$$

The quantity Q is the matrix of frequency domain generalized forces that is computed for the given frequency and phase of the forcing term. Note that, from Eq.(VI.3) , the matrix Q is simply $i\omega$ times the Laplace transform (with $s = i\,\omega$) of the generalized derivative matrix A.

Stability

In the stability analysis, we take $F_0 = 0$, and consider the temporal response to initial conditions $q = \dot{q} = 0$,for $t < 0$; $q = 0$,$\dot{q} = v_0$ for $t = 0+$. This initial value problem can be solved formally by Laplace transforms (which we denote by L[]), since the aerodynamic forces are in the form of a convolution. The resulting solution for $\bar{q}(s) = L[q(t)]$, at a fixed interblade phase angle, is

$$\bar{q}\,(s) = [\, M\,s^2 + C\,s + K - Q(s)\,]^{-1}\,M\,v_0 \qquad \text{(VI.7)}$$

where $Q(s) = s\,L[A]$. The Laplace integral definition of Q is convergent everywhere in $Re(s) \geq 0$, but not in $Re(s) < 0$. In order for residue theory to be useful in finding the inverse transform of $\bar{q}$ (ie. q(t)), we must define Q(s) in $Re(s) < 0$ as the analytic continuation from the right half s plane. If this step is made, then stability can be determined simply by finding that root s_c of the determinate,

$$D(s) = \det [\, M\,s^2 + C\,s + K - Q(s)\,] = 0 \qquad \text{(VI.8)}$$

which has the largest real part. If $Re(s_c) > 0$ the rotor is unstable. If $Re(s_c) < 0$ then the rotor is stable for the given phase angle. In general, each interblade phase angle must be examined independently to find the most unstable collective mode.

The procedure used to do the analytic continuation of Q(s) involves simple interpolation on the imaginary axis. The generalized forces are computed at N_ω user chosen frequencies ω_k , $k = 1$, N_ω (which typically are near one or more invacuum natural frequencies.) Within this frequency band Q(s) is defined by an interpolant,

$$Q(s) \cong \Sigma_i\,[a_i\,G_i(s)\,] \qquad \text{(VI.9)}$$

where the G_i are analytic shape functions, and the a_i are coefficients determined from the interpolation conditions at the knots $s_k = i\,\omega_k$

$$\Sigma_i\,[a_i\,G(s_{k)_i}\,] = Q(s_k) \qquad \text{(VI.10)}$$

Although many different shape functions could be used, the ones chosen here are,

$$G_i = [1, s, s^2, \ldots, s/(s+\beta_{i-3})] \qquad \text{(VI.11)}$$

where β_{i-3} are real positive numbers selected to scale with the chosen frequencies. These functions have the property that the roots of Eq(VI.8) can be found by any standard complex eigensolver on an extended state space of dimension $N_s = N_{mode} \max(2, N_\omega - 1)$ consisting of the original states q, $\dot{q}$ plus (if $N_\omega > 3$) extra 'aerodynamic states' $G_k\, q$; $k = 4, \ldots, N_\omega$.

The eigenvalues so determined will be N_s in number, and nonconjugate. Only those roots that fall within the circle of diameter $\omega_{N_\omega} - \omega_1$ centered at $i\,[\omega_{N_\omega} + \omega_1] / 2$ are admitted. How many are found, of course, depends on how broad the original frequency band is. A simple strategy is to partition the range of invacuum natural frequencies included in the model, sweeping through the set successively with $N_\omega = 3$. This does not increase the size of the state space for any one band, and usually leads to N_{mode} acceptable roots. If this procedure is used repetitively to find a critical (or flutter) point, the frequency and interblade phase angle bands that need to be investigated can be narrowed very quickly as more is learned about the system.

Table 1.

PURDUE MODEL BLADE GEOMETRY

$\bar{r}$	$\Delta\beta$	b/r_t	C_{L_D}
.275	0.396	.333	0.
.3475	0.309	.333	0.
.4200	0.241	.333	0.
.4925	0.180	.333	0.
.5650	0.122	.333	0.
.6375	0.075	.333	0.
.7100	0.014	.333	0.
.7825	-0.034	.333	0.
.8550	-0.086	.333	0.
1.0	-0.163	.333	0.

Table 2

NACA 109622 GEOMETRY

$\bar{r}$	$\Delta\beta$(rad)	b/r_t	C_{L_D}
.25	0.445	.24	0.
.35	0.315	.24	0.
.45	0.227	.24	0.
.55	0.140	.24	0.
.65	0.061	.24	0.
.75	0	.24	0.
.85	-0.052	.24	0.
.95	-0.104	.24	0.
1.0	-0.131	.24	0.

Table 3

SR2 GEOMETRY

$\bar{r}$	$\Delta\beta$(rad)	b/r_t	C_{L_D}
.3	.262	.3	-.036
.4	.215	.3	.091
.5	.150	.298	.150
.6	.087	.296	.173
.7	.024	.292	.145
.8	-.028	.284	.091
.9	-.079	.258	.041
.95	-.096	.226	.018
1.0	-.122	.102	.009

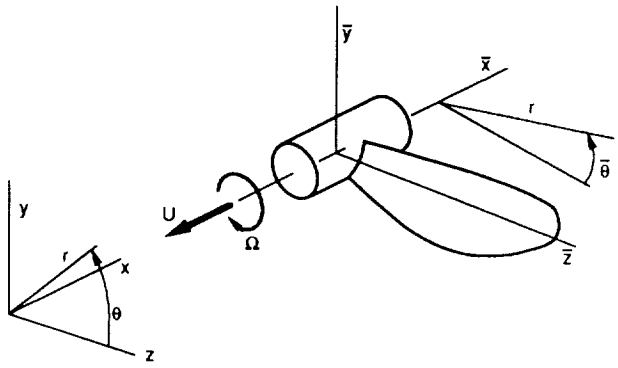

Figure 1. - Coordinate systems.

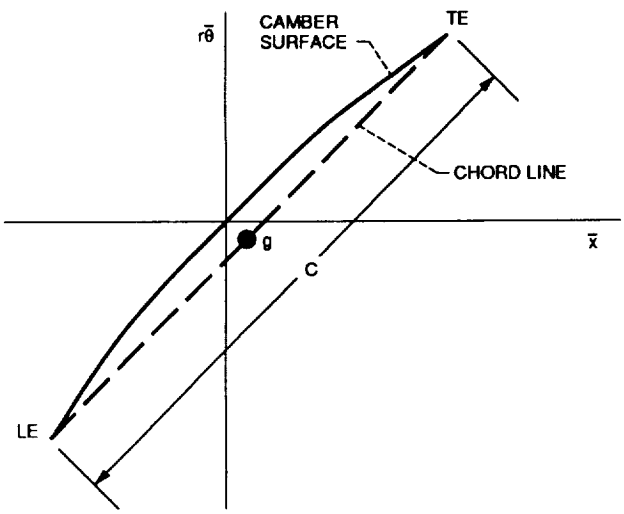

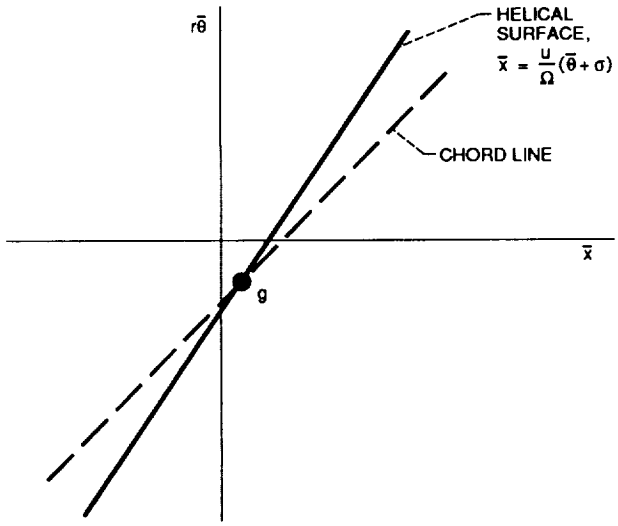

Figure 2. - Helical surface construction.

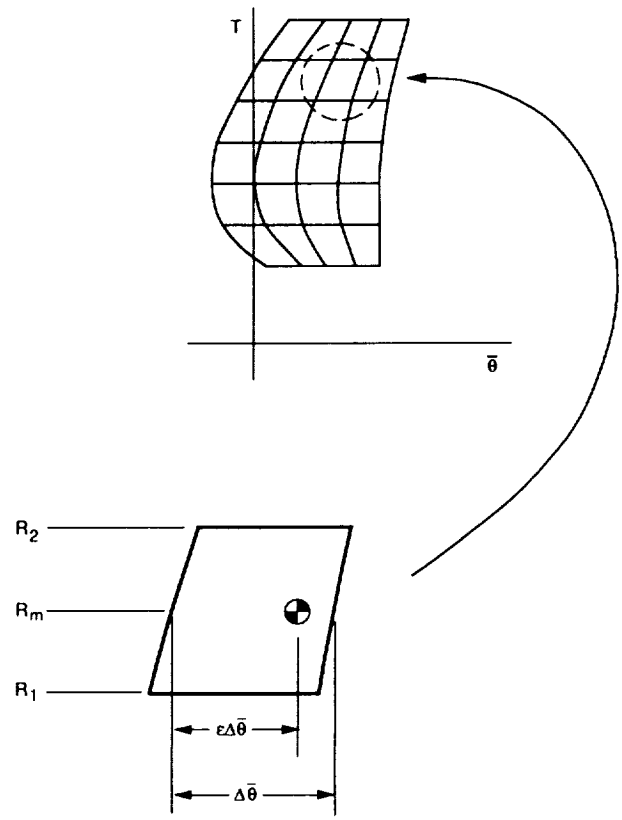

Figure 3. - Blade paneling and control point placement.

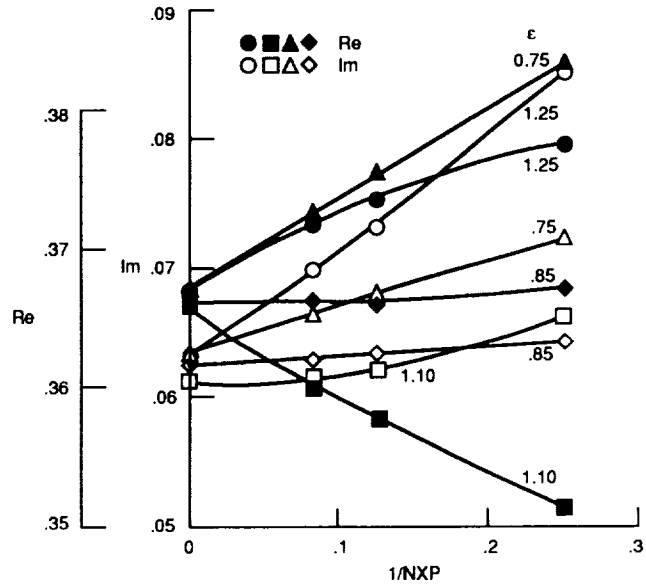

Figure 4. - Convergence of sectional thrust at $\bar{r} = 0.8$ for vibrating propeller.

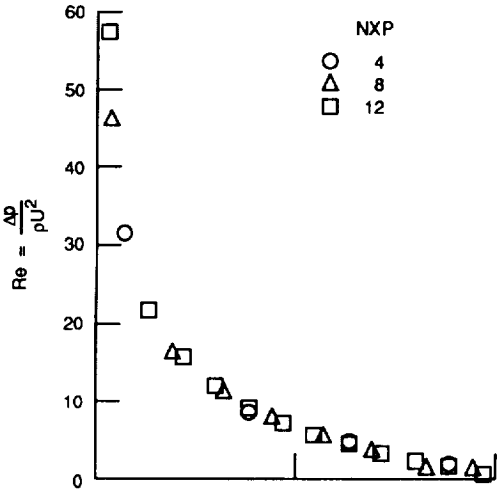

(a) Real part.

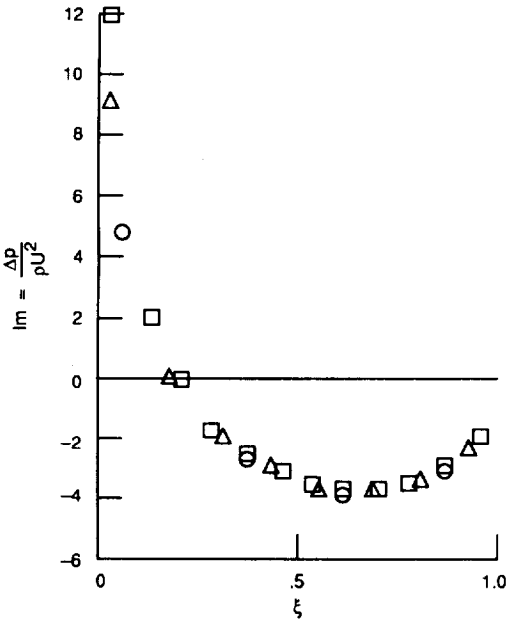

(b) Imaginary part.

Figure 5. - Convergence of the pressure distribution at $\bar{r} = 0.8$, $\varepsilon = 0.85$.

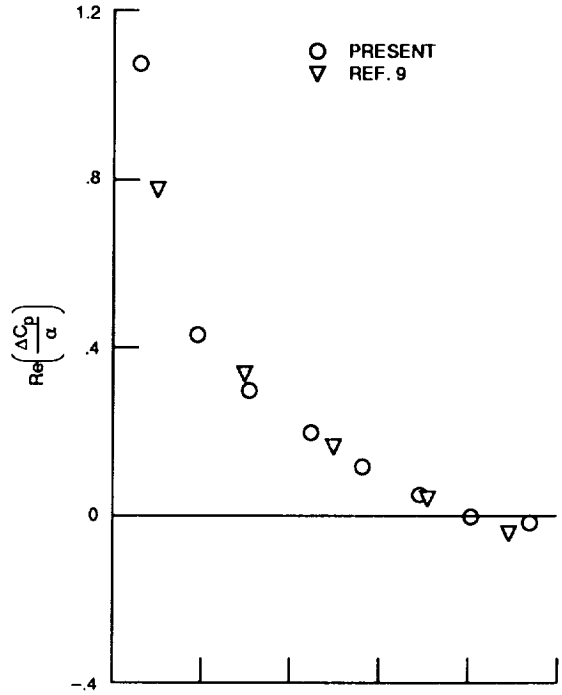

(a) Real part.

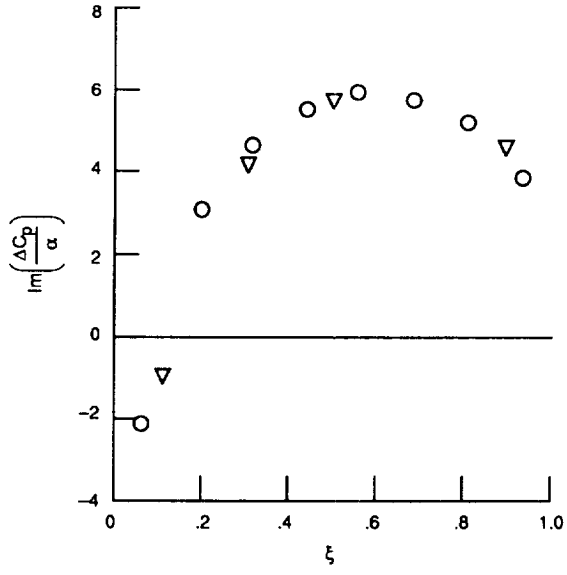

(b) Imaginary part.

Figure 6. - Midspan pressure distribution for a pitching wing.

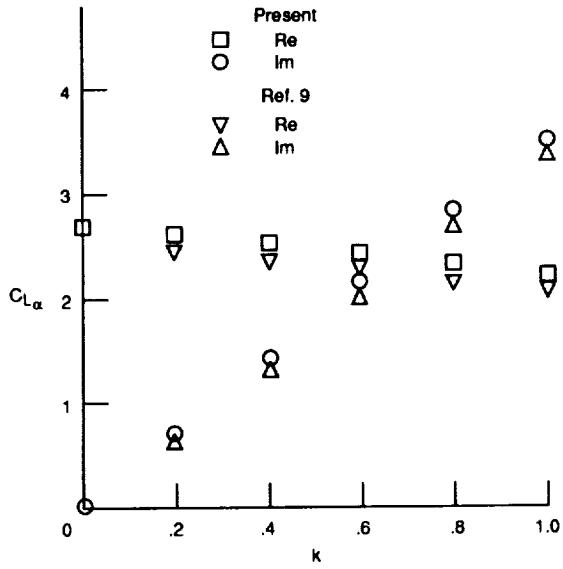

Figure 7. - Unsteady lift for a pitching wing.

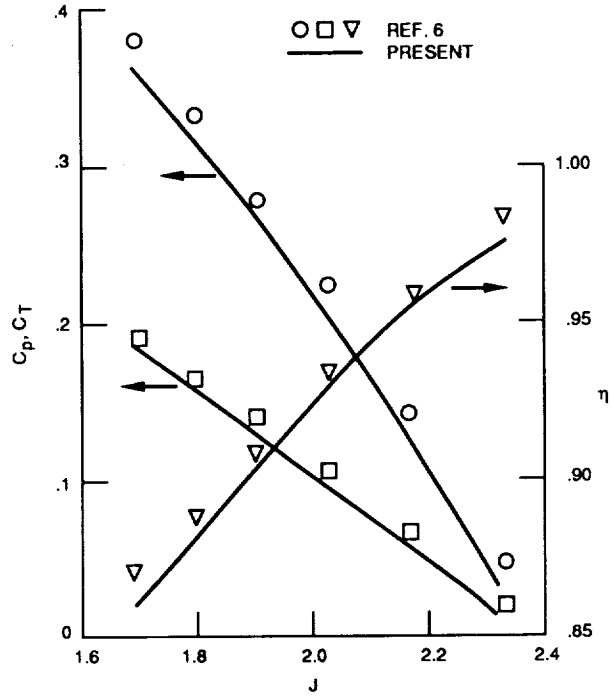

Figure 9. - Performance characteristics of the NACA 109622.

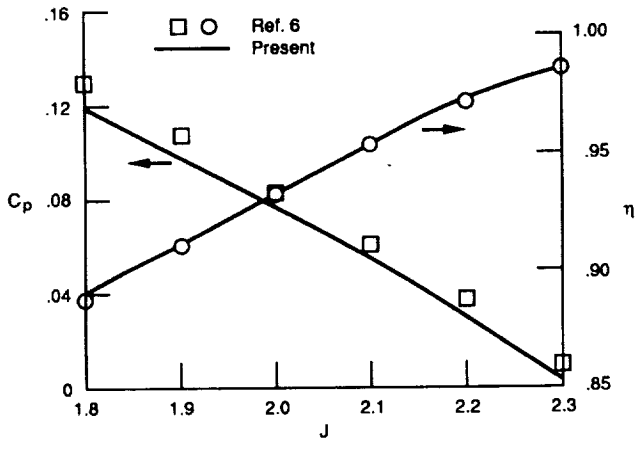

Figure 8. - Performance characteristics of the Perdue Model blade.

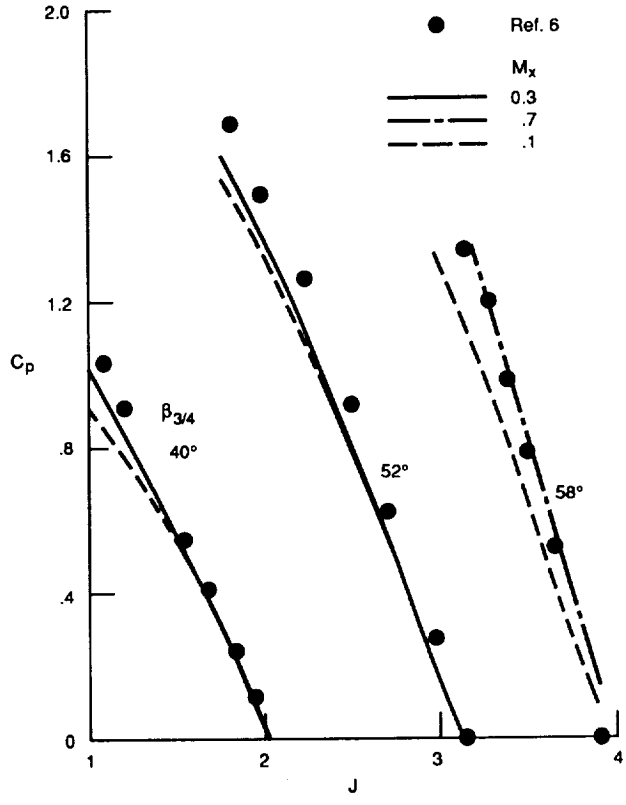

Figure 10. - Performance characteristics of the SR2.

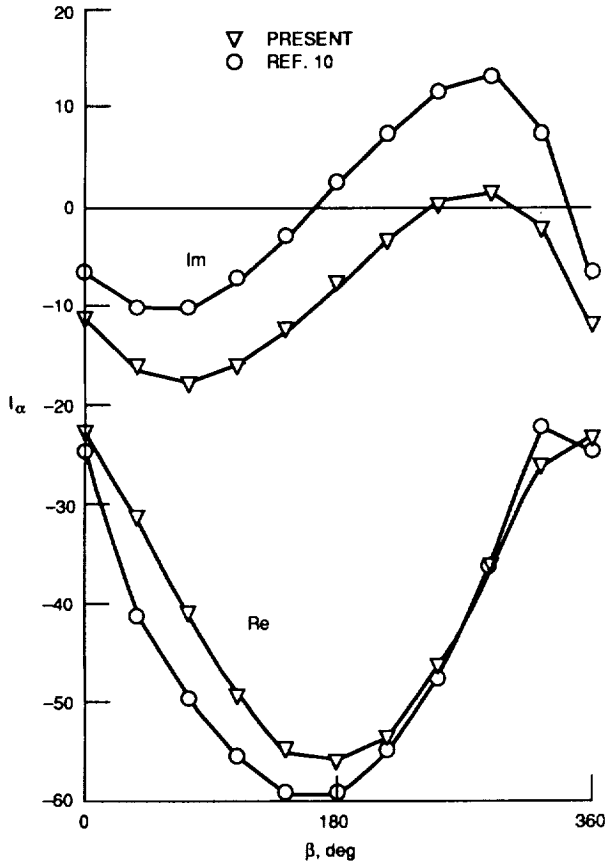

Figure 11. - Torsional lift at $\bar{r} = 0.6$ for a 10 bladed fan.

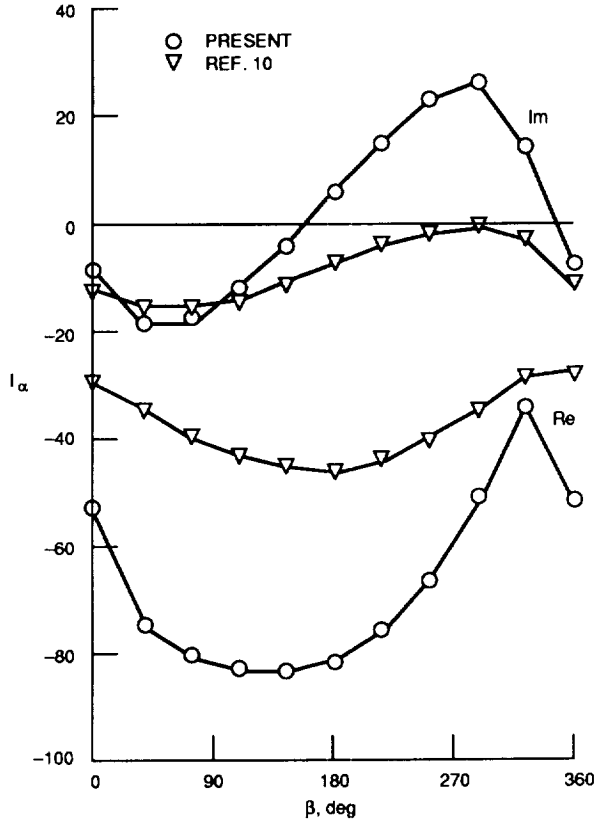

Figure 12. - Torsional lift at $\bar{r} = 0.9$ for a 10 bladed fan.

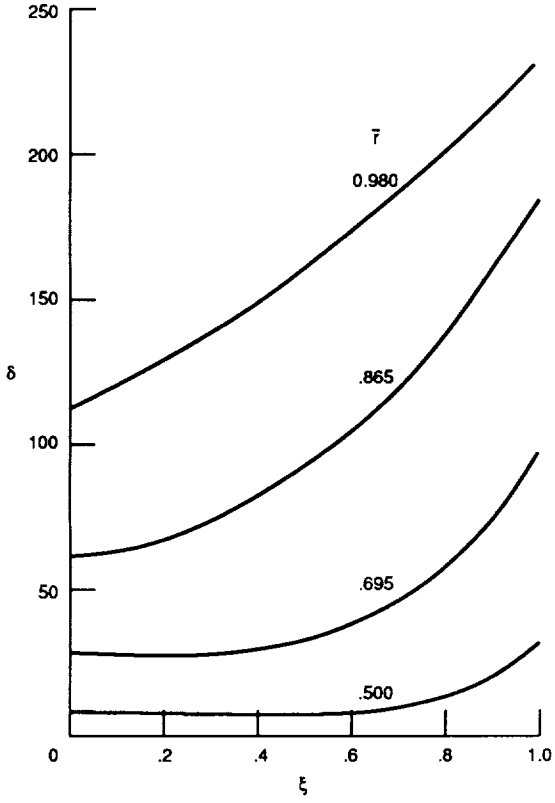

Figure 13. - Mode 1 normal displacements of the SR3.

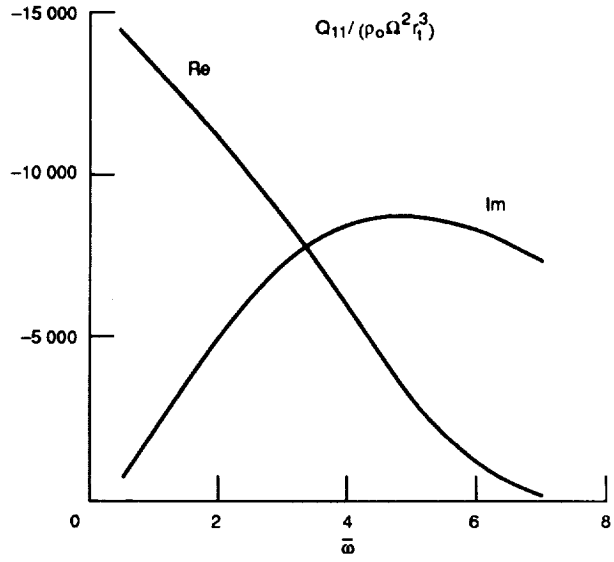

Figure 14. - Generallzed aerodynamic force for the SR3.

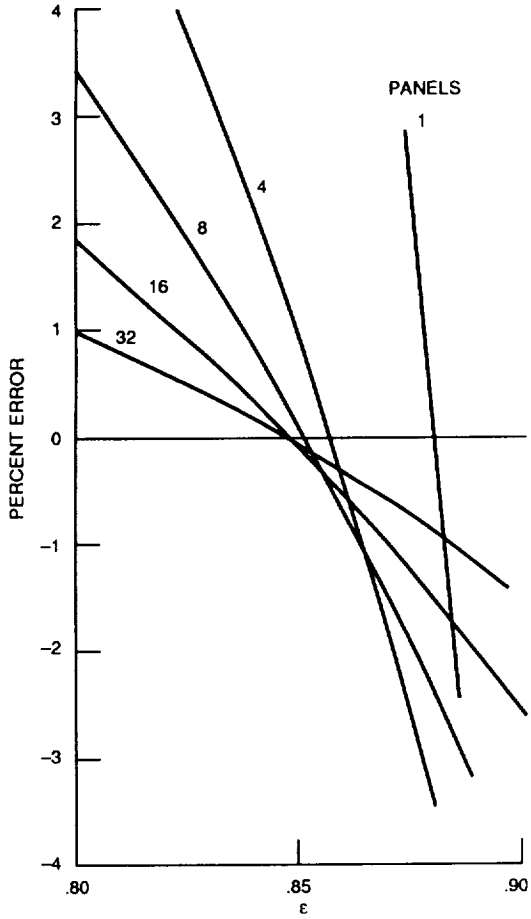

Figure V.1. - Convergence of net circulation.

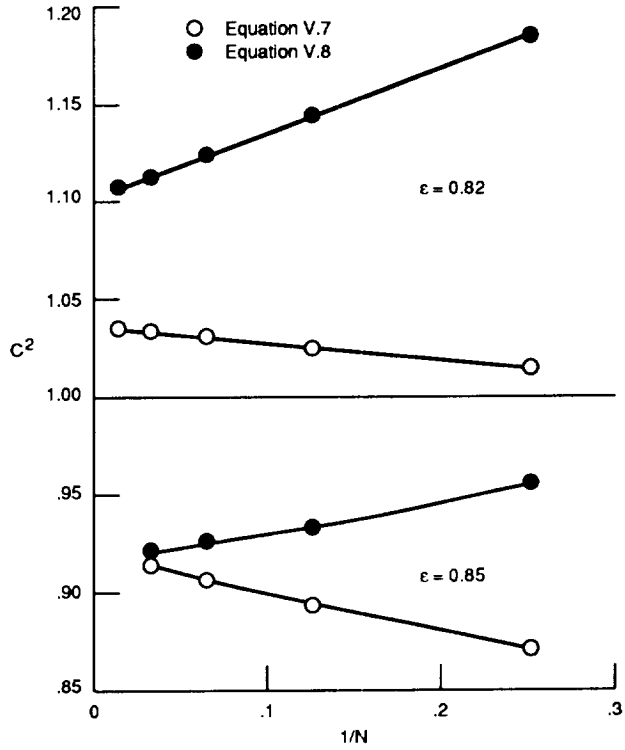

Figure V.2. - Behavior of singularity strength as N increases.

NASA
National Aeronautics and Space Administration

Report Documentation Page

1. Report No.	2. Government Accession No.	3. Recipient's Catalog No.
NASA CR-4302		

4. Title and Subtitle	5. Report Date
An Unsteady Lifting Surface Method for Single Rotation Propellers	July 1990
	6. Performing Organization Code

7. Author(s)	8. Performing Organization Report No.
Marc H. Williams	None (E-5428)
	10. Work Unit No. 505-62-4D

9. Performing Organization Name and Address	11. Contract or Grant No.
School of Aeronautics and Astronautics Purdue University West Lafayette, Indiana 47907	NAG3-499
	13. Type of Report and Period Covered Contractor Report Final

12. Sponsoring Agency Name and Address	14. Sponsoring Agency Code
National Aeronautics and Space Administration Lewis Research Center Cleveland, Ohio 44135-3191	

15. Supplementary Notes

Project Manager, George L. Stefko, Structures Division, NASA Lewis Research Center. This work has been supported under Grant NAG3-499 from NASA Lewis Research Center. The Propulsion Systems Division, Propeller and Acoustics Technology Branch, and the Structures Division, Structural Dynamics Branch sponsored this work.

16. Abstract

The present report describes the mathematical formulation of a lifting surface method for evaluating the steady and unsteady loads induced on single rotation propellers by blade vibration and inflow distortion. The scheme is based on three dimensional linearized compressible aerodynamics and presumes that all disturbances are simple harmonic in time. This approximation leads to a direct linear integral relation between the normal velocity on the blade (which is determined from the blade geometry and motion) and the distribution of pressure difference across the blade. This linear relation is discretized by breaking the blade up into subareas (panels) on which the pressure difference is treated as approximately constant, and constraining the normal velocity at one (control) point on each panel. The piece-wise constant loads can then be determined by Gaussian elimination. The resulting blade loads can be used in performance, stability and forced response predictions for the rotor. The report is divided into two sections and appendices. Section 1 deals with mathematical and numerical aspects of the method. Section 2 presents a selection of results obtained from the method, The appendices include various details of the derivation that were felt to be secondary to the main development in Section 1.

17. Key Words (Suggested by Author(s))	18. Distribution Statement
Linearized unsteady flows; Small disturbance theory; Propeller blade loads; Panel methods; Aeroelastic applications	Unclassified – Unlimited Subject Category 02

19. Security Classif. (of this report)	20. Security Classif. (of this page)	21. No. of pages	22. Price*
Unclassified	Unclassified	63	A04

NASA FORM 1626 OCT 86

*For sale by the National Technical Information Service, Springfield, Virginia 22161

NASA-Langley, 1990